HELLENIC REPUBLIC
National and Kapodistrian University of Athens
Faculty of Geology and Geoenvironment
Dynamic Tectonic and Applied Geology

DYNAMIC TECTONIC AND APPLIED GEOLOGY

MSc THESIS

TECTONOSTRATIGRAPHY OF HERAKLIA ISLAND, BASED ON GEOLOGICAL MAPPING, STRUCTURAL ANALYSIS AND LA-ICP-MS DETRITAL ZIRCON DATING.

SOFIA LASKARI

21328

EXAMINING COMMITTEE

Stylianos Lozios (Supervisor) (National and Kapodistrian University of Athens)

Daniel Fritz Stockli, Professor (Jackson School of Geosciences, UT Austin)

Konstantinos Soukis, LTS (National and Kapodistrian University of Athens)

Athens, 2017

ACKNOWLEDGEMENTS

I would like to express my great appreciation to my research supervisors Ass. Prof. Dr. Stylianos Lozios and Prof. Dr. Daniel Stockli for their guidance and support during my research work. My grateful thanks to Prof. Dr. Daniel Stockli for his efficient assistance during sample preparation and the dating of the zircons involved in this study.

I would also like to extend my thanks to my co-supervisor Dr. Konstantinos Soukis for his advice, support, the valuable comments on this thesis, and the helpful discussions thoughout my research.

My special thanks to the Ph.D. student George Papantoniou and MSc student Myrto Kalogeraki for their encouragement throughout my years of study.

Finally, I would like to thank my family for their support during my research.

CONTENTS

1. INTRODUCTION

After the formation of the Hellenides chain, kinematics in the upper plate since 35 Ma, has been controlled by the fast southward retreat of the Hellenic subduction zone, and as a result the kinematics conditions changed from compressional to extensional in the back arc domain (Rocke et al., 2016, Maliverno and Ryan 1986, Jolivet and Faccenna 2000, Jolivet et al., 2008, Jolivet and Brun 2010). This evolution led to the development of large – scale extensional detachment faults in the Aegean area. Four main extensional systems were formed: the North Cycladic Detachment System (NCDS) and the N-PDS (Naxos-Paros Detachment System) that are associated with top-to-the NE kinematics, and the West Cycladic Detachment System (WCDS) and the South Cycladic Detachment System (SCDS) with top-to-the SW and top-to-the S shearing respectively. All detachment faults were active during greenschist metamorphism and resulted in the exhumation of metamorphic core complexes.

The best examples of such core complexes are the islands of Ios and Naxos (Huet et al., 2009, Lister et al., 1984) that were exhumed below the SCDS and N-PDS respectively. On both islands the pre-Alpine basement and the Cycladic Blueschist Unit are observed. The rocks of the CBU in Naxos island underwent an HP metamorphic event at about ~50 Ma (Urai et al., 1990, Durr et al., 1978), followed by greenschist to amphibolite-facies paragenesis and partial melting in the Miocene (Jansen and Schuiling 1976, Buick and Holland 1989, Wijbrans et al., 1990). Exhumation of the CBU rocks commenced at ~20 Ma, according to U-Pb data on zircon (Keay 2001, Ring et al., 2010), and was accommodated by the top-to-the-north Naxos-Paros Detachment System (N-PDS) (Menant et al., 2016, Brichau et al., 2006, Seward et al., 2009, Urai et al., 1990, Gautier et al., 1993). On the other hand, on Ios island, metamorphism was recorded at about 40-50 Ma and 25-30 Ma for HP/LT and LP/HT event, respectively (Huet et al., 2009, Van der Maar and Jansen 1983, Andriessen et al., 1987, Baldwin and Lister 1998). The presence of top-to-the-north and top-to-the-south kinematics are still a matter of debate. Foster and Lister 1999a, reported that these structures are related to post-orogenic deformation, suggesting a symmetrical model of extension on Ios island. However, the reexamination of field relations suggested that the top-to-the-south kinematics correspond to an Eocene pre-extension stage, and were reworked by top-to-the-north extensional shear sense (Huet et al., 2009, Huet et al., 2010, Jolivet et al., 2012).

The island of Heraklia, located between Ios and Naxos, is an ideal study area in order to compare the relations between deformation and metamorphism of this island with those which were described on Ios and Naxos islands. This study provides new U-Pb data on detrital zircon combined with field observations and structural analysis.

2. GEOLOGICAL SETTING

2.1. HELLENIC ARC

The Hellenic subduction zone is the most seismically- tectonically active system in the Mediterranean region (fig. 1). According to GPS data, the northeastward subduction of the east Mediterranean oceanic lithosphere beneath the southern portion of the Hellenic trench, occurs at ~35 mm/y (Kahle et al., 2000, McClusky et al., 2000, Nyst and Thatcher 2004). The subduction front trends NW-SE in the Ionian side, whereas in the Levantine side it trends NE-SW, and is marked by the Hellenic trench, which corresponds to a succession of elongate trenches reaching the depth of 5km (Finetti et al., 1990).

To the northwest, the Hellenic subduction is seperated by the dextral Kephalonia Transform Zone, which was formed at about 6-8 Ma, as a consequence of different subduction rates between the northern and southern Hellenides (Royden and Papanikolaou, 2011).

To the north, the Hellenic arc is bounded by the North Aegean Trough, which represents a transtensional tectonic basin, and it was formed by a combination of the retreat of the Hellenic subduction zone and the propagation of the dextral strike-slip North Anatolian Fault (NAF) since Mio-Pliocene boundary (~5 Ma) (Armijo et al., 1999). The NAF is connected to the Hellenic trench through the Central Hellenic Shear Zone (CHSZ). This zone represents a transtesional shear zone that crosses older structures of the Hellenic thrust belt (Papanikolaou and Royden, 2007).

To the northeast, the Hellenic arc is bounded by the West Anatolian Shear zone in a NW-SE direction, accommodating a slab tear (sub-vertical rupture within the subducting slab) to the crust and appears to have been formed between 16 and 8 Ma (Jolivet et al., 2012). Another slab tear has been proposed to exist below the Corinth Gulf, which facilitates the junction between the North Anatolian Fault and the Hellenic trench through the Central Hellenic Shear zone and the Kefalonia fault (Jolivet et al., 2012, Jolivet et al., 2015).

Finally, based on geodynamic analysis, the segmentation of the Hellenic trench, the development of the Central Hellenic Shear zone and the North Aegean Trough, are all related and they are driven from the rapidly southward slab retreat (Jolivet et al., 2012).

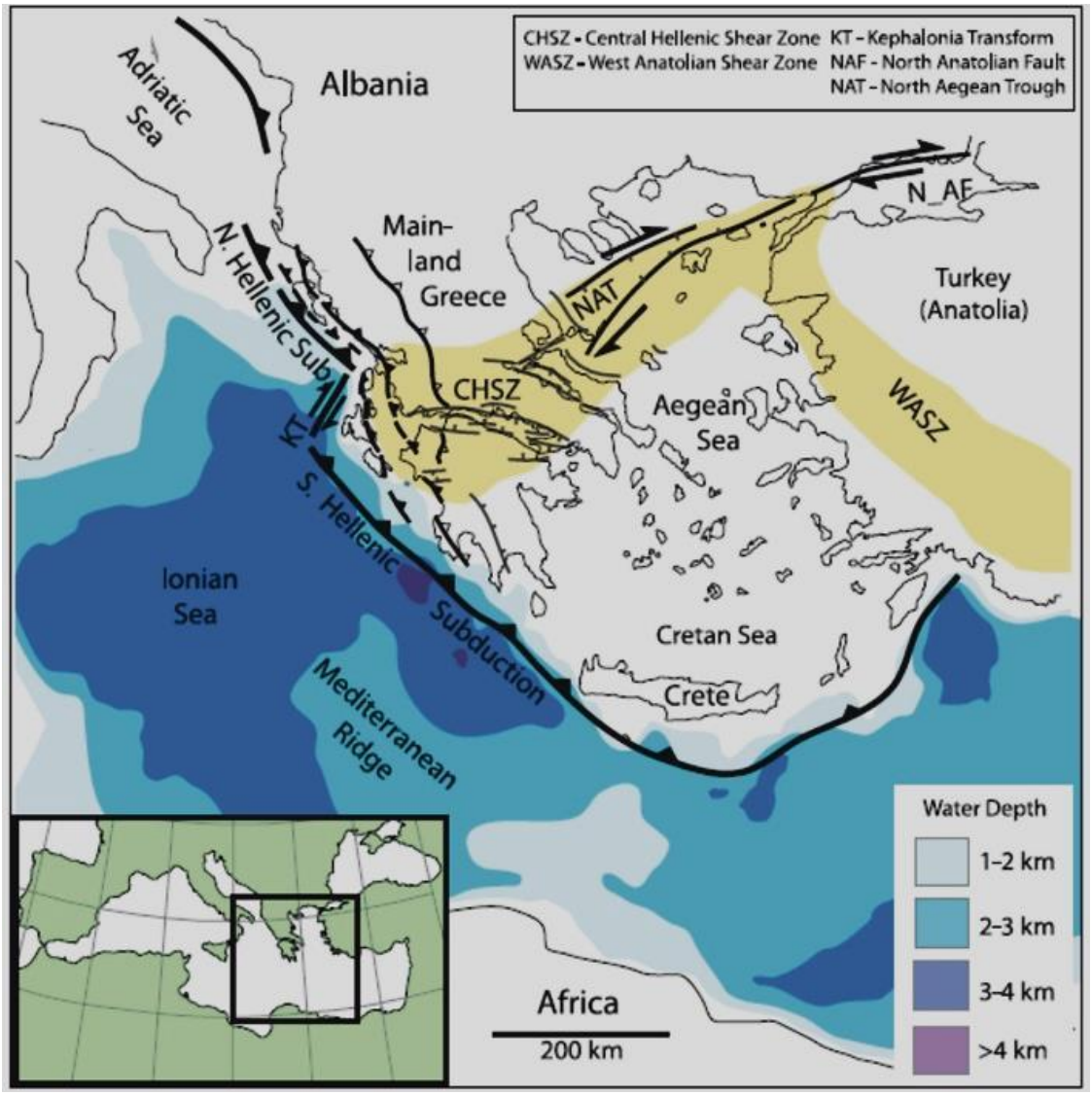

Figure 1: Tectonic map, representing the Hellenic subduction zone and the active trenches. The two shear zones, which bound the northwestern and northeastern margins of the Hellenic arc, are depicted in light yellow (modified after Royden and Papanikolaou, 2011).

2.2. Geodynamic Evolution of the Hellenides

The convergence of the Africa- Europe since the late Mesozoic has led to the formation of stacked nappes within an accretionary wedge in the Aegean. These nappes represent the upper crustal portions that detached from the subducting oceanic or continental plate and formed an orogenic wedge with a migration from NE to SW (van Hinsbergen et al., 2005).

According to Papanikolaou (1989a, 1997, 2009) the paleographic organization of the Hellenides involved a number of tectostratigraphic terranes, including four oceanic basins and five continental fragments (fig. 2). All oceanic terranes are considered to be parts of the Tethys ocean that closed throughout Mesozoic - Cenozoic time and

represent the ophiolite suture zones within the Hellenides, and the continental fragments including the pre-Alpine basement covered by shallow-water carbonate platforms of Mesozoic- early Cenozoic represent parts of the Gondwanian margin, which were drifted northwards and accreted to the European margin, except for the most internal terrane (H9) that probably belongs to the European margin (Papanikolaou, 1989, 1997). The present day relic of the Tethys ocean in the Eastern Mediterranean could be considered as a future terrane (H0), which started its subduction the past 10-5 Ma. However, the number of these terranes is still a matter of strong debate.

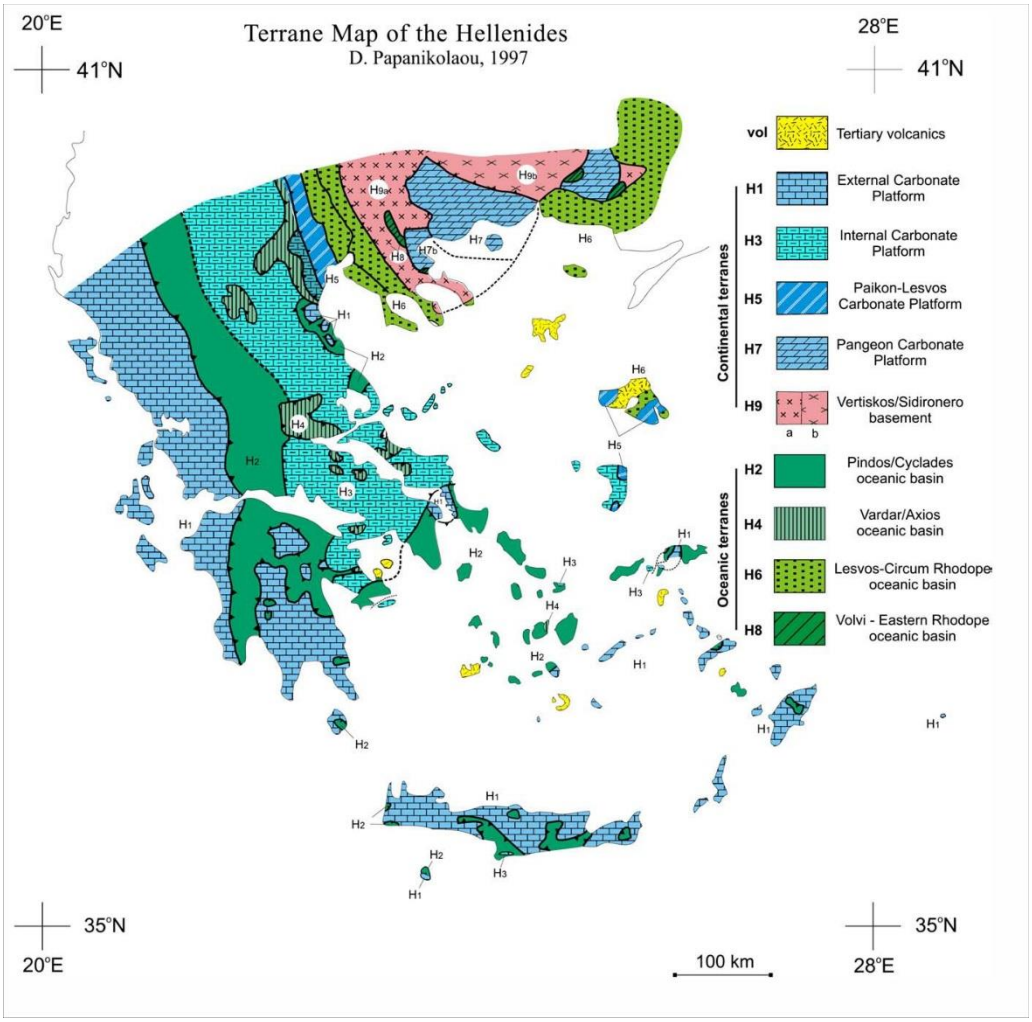

Figure 2: Tectonostratigraphic terrane map of the Hellenides (Papanikolaou, 1997)

Another paleographic model of the Hellenides involves six domains, which include from north to south: i. *Vardar-Izmir oceanic domain*, ii. the *Pelagonian-Lycian domain*, iii. the *Pindos oceanic domain*, iv. the *Gavrovo-Tripoliza domain*, v. the *Ionian* and the *pre-Apoulian domain* and vi. the *East Mediterranean oceanic domain* (fig. 3) (Ring et al., 2010).

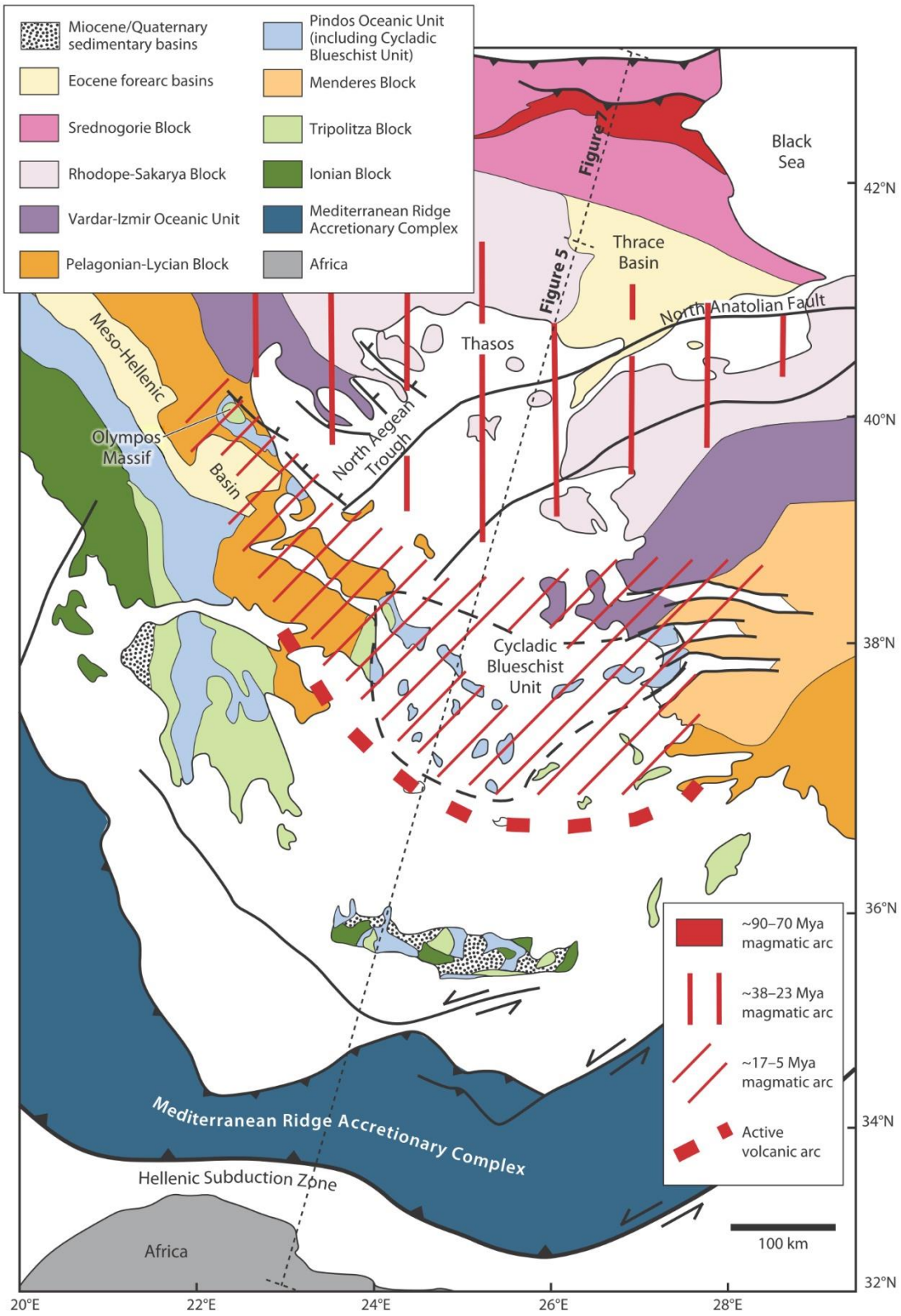

Figure 3: Tectonic map of the Aegean, representing all the nappes, which form the Hellenides, and the main tectonic zones (Ring et al., 2010).

The *Vardar-Izmir* was the first domain that subducted beneath the Srednogorie and Rhodope-Sakarya blocks to the north during Late Jurassic to Cretaceous, and includes mainly ophiolitic rocks and oceanic sediments. The subduction of the Vardar-Izmir oceanic unit had as a result the formation of a volcanic arc in southern Bulgaria at ~90-75 Ma (von Quadt et al., 2005, Ring et al., 2010).

The *Pelagonian domain* and the overlying Jurassic ophiolites of Vardar ocean were underthrusted in the late Jurassic to Paleogene. The Pelagonian unit consists of a Carboniferous continental basement, which is overlain by Paleozoic and Mesozoic sedimentary rocks. Parts of this unit were metamorphosed under blueschist facies between 125-85 Ma (Lips et al., 1999, Ring and Layer 2003).

The *Pindos domain* generally a deep marine area that involves both oceanic and continental platform sediments, which were subducted in the Eocene. Parts of the Pindos domain were metamorphosed under blueschist facies and locally reached the eclogite facies, exposed today in the Cyclades and Evia (Cycladic Blueschist Unit). The Cycladic Blueschist Unit (CBU) is a Mesozoic sequence of marbles and metapelites underlain by a Carboniferous basement of orthogneiss and schists, (Papanikolaou 1976, 1977, 1978, 1979, Durr et al., 1978, Ring and Layer 2003, Ring et al., 2010). The main argument for the correlation between the CBU and the Pindos unit is their similar tectonic position between the nappes Gavrovo-Tripoliza and Pelagonian. According to recent views (van Hinsbergen and Schmidt 2012; Tremblay et al., 2015) the Pindos domain is not oceanic but it represents a deep marine basin separating the Pelagonian and the Gavrovo-Tripolitza domain.

The *Gavrovo-Tripoliza* domain consists of a thick carbonate sequence of Triassic to Eocene age, and is overlain by a Late Eocene to Early Oligocene flysch (Jacobshagen 1986). The subduction of the Gavrovo-Tripoliza block started after the deposition of the flysch at about 35-30 Ma (Thomson et al., 1998a, Sotiropoulos et al., 2003). This unit crops out in Peloponnese and Crete as the Gavrovo-Tripoliza nappe, and also in the Mount Olympos, south Evia (Almyropotamos) and Samos (Kerketeas) as a metamorphic equivalent, forming tectonic windows below the overlying Cycladic Blueschist Unit (Godfriaux 1968, Dubois and Bignot 1979, Theodoropoulos 1979, Papanikolaou 1979, Ferriere 1982, Papanikolaou 1986, Godfriaux and Ricou 1991, Ring et al., 1999b, Shaked et al., 2000). Below the Gavrovo-Tripoliza unit the Phyllite-Quartzite unit, consisting of volcanites, marbles and lenses of higher-grade basement rocks. The Phyllite-Quartzite Unit probably represents the base of the Gavrovo-Tripoliza domain (Van Hinsbergen et al., 2005b).

The *Ionian* and the *pre-Apoulian* domains represent the outermost nappes of the Hellenides, and consist of Mesozoic carbonates that are overlain by late Eocene-Miocene turbidites (Papanikolaou 1986). The Ionian unit was subducted at the same time with the Gavrovo-Tripoliza unit, and was metamorphosed in depth into Plattenkalk unit, which is exposed today in Peloponnese and Crete. The Plattenkalk unit represents the deepest tectonic unit of the external Hellenides and it is still

unknown what underlies this unit. During the Miocene to Early Pliocene the Ionian unit overthrusted the pre-Apoulian platform.

The *East Mediterranean* domain represents an oceanic Triassic crust (~250-200 Ma) (Van Hinsbergen et al., 2005), which started its subduction during the early or middle Miocene (Underhill 1989, Le Pichon et al., 2002) and it is still subducting. This domain includes two basins, the Ionian and the Levantine basin, which are located in the north-western Greece and in the south-eastern Greece respectively. South of Crete, the East Mediterranean ridge is formed due to the total subduction of the oceanic crust, and the leading edge of the African passive margin into the subduction zone (Ring et al., 2010).

A reconstruction of the Hellenides is presented in cross sections starting from ~80 Ma to the present (Ring et al., 2010) (fig. 4). At 80 Ma, after the subduction of the Vardar-Izmir oceanic domain and parts of the Pelagonian block, a volcanic arc was formed in the Rhodope- Sakarya block. At that time HP- metamorphism occurred in the Vardar-Izmir and Pelagonian domains. At about 50 Ma the Pindos oceanic domain has already entered the subduction zone, and the Cyclades were metamorphosed in eclogite to blueschists-facies conditions and were exhumed within the subduction zone. At 35 Ma the Tripolitza continental block was subducted and a relative magmatic arc was developed in the Northern Aegean. At this stage the slab started to retreat faster and back-arc extension was accommodated along detachment faults. From 23 to 15 Ma, as slab retreat continued, back arc extension and the activity of the detachments reached a peak in the entire Aeagean area. That time the Hellenic trench moved outboard and the magmatic arc was developed in Cyclades. HP rocks started to exhume in extrusion wedges in Crete. Presently, extension localized in the Cretan Sea and the North Anatolian fault entered the Aegean domain, causing alkaline-subalkaline volcanism.

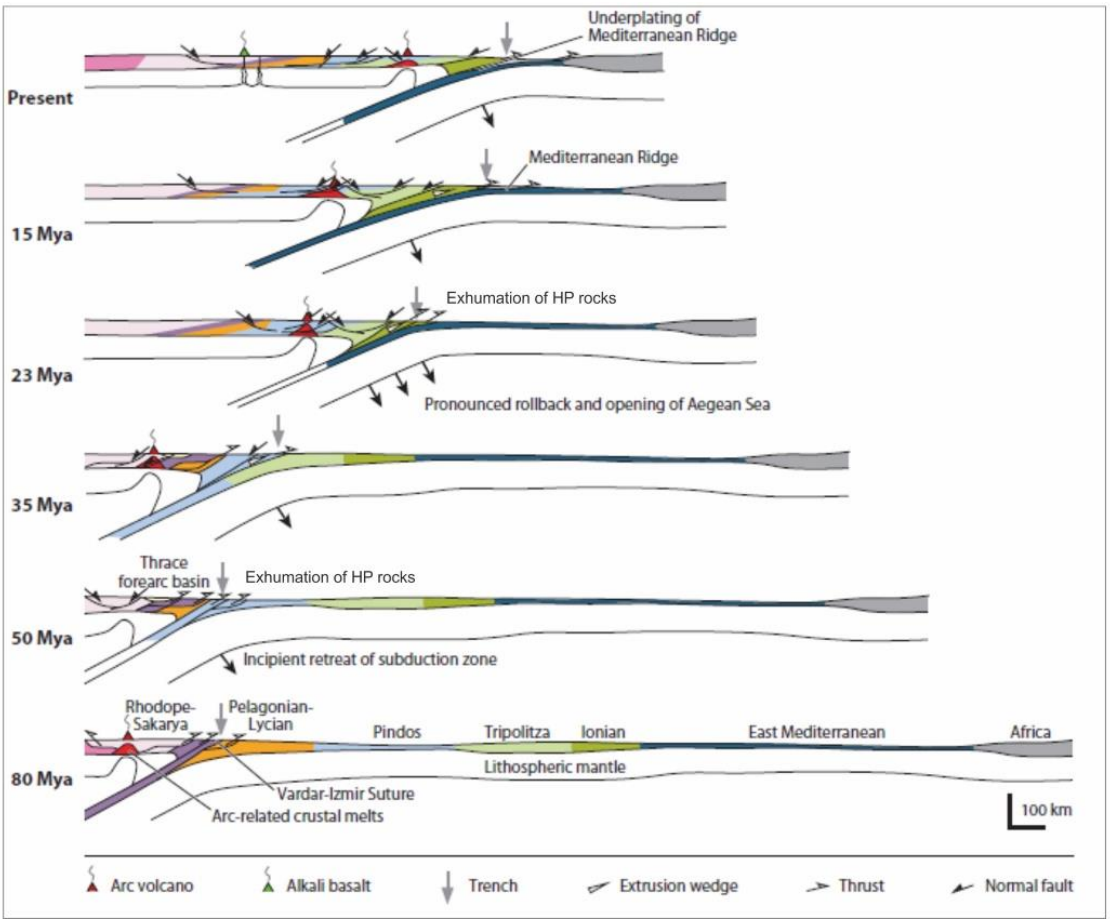

Figure 4: A reconstruction of the Hellenic subduction system from 80 Ma to the present (Ring et al., 2010).

2.3 Tectonic evolution in the Aegean area

After the formation of the Hellenides, kinematics in the upper plate since 35 Ma, has been controlled by the fast southward retreat of the subduction zone, and as a result the kinematic boundary conditions changed from compressional to extensional in the back arc area (Maliverno and Ryan 1986, Jolivet and Faccenna 2000, Jolivet et al., 2008, Jolivet and Brun 2010). A retreat or roll-back of the slab, commonly happens when the rate of the overriding plate's convergence with the trench is smaller than the subduction rate. Subsequently, an horizontal extension occurs in the upper plate (fig. 5) (Dewey and Bird 1970, Garfunkel et al., 1986, Royden 1993, Lonergan and White 1997, Ring et al., 2010). The Hellenic subduction system is a well-preserved example of a retreating subduction zone that caused the N-S extension in Aegean region.

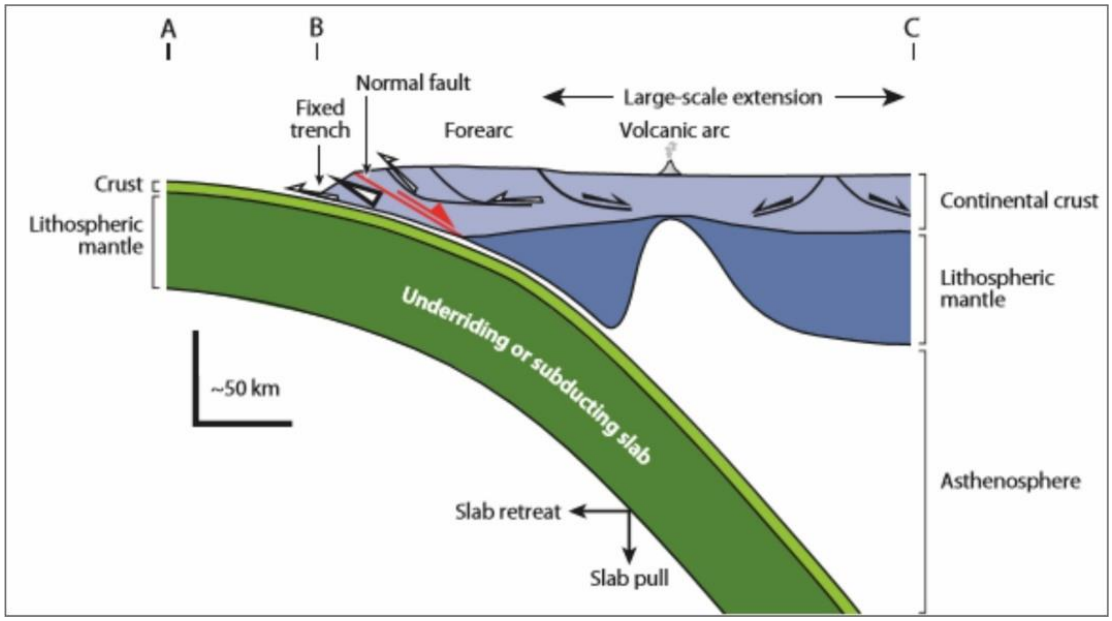

Figure 5: Sketch indicating slab retreat defined by a subduction rate (AB) that is greater than the convergence rate (AC) (Royden 1993). Extrusion wedges are formed at the edge of the overriding plate and the top is marked by a normal fault (red), whereas, the base is marked by a thrust fault (Ring et al., 2010).

Even though many investigations have been carried out, the age of the first back arc extension in the Aegean area is still debated. Early interpretations, suggested that extension started as late as 13 Ma (Le Pichon and Angelier, 1981b) or even 5 Ma (Mc Kenzie, 1978). However, field observations proposed earlier ages in the Early or Middle Miocene (Mercier et al., 1976) based on unconformable marine deposit, which were found in Naxos and Evia (Guernet 1971, Angelier et al., 1978, Katsikatsos et al., 1981, Sanchez-Gomez et al., 2002, Kuhlemann et al., 2004, Ring et al., 2010, Jolivet et al., 2012). Ring et al., 2010, suggested that the extension started at about 23 Ma, according to the earliest sediments that were found in the Aegean islands.

However, some authors mentioned that if the Rhodope massif is considered as part of the Aegean, then, extension must have started earlier than 35 Ma (fig. 6) (Brun and Sokoutis, 2010). According to U-Pb ages on zircon, the Rhodope massif has undergone a HP metamorphism with locally ultra-HP conditions (Liati et al., 2002, Bonev et al., 2006, Bauer et al., 2007) and was followed by a MT-MP metamorphirsm in Paleocene times. In central Rhodope, these rocks were exhumed in Eocene time (~55 Ma) below ductile- brittle detachments with top-to-the NE kinematics (Burg et al., 1996, Bonev et al., 2006), whereas, in southern Rhodope, the exhumation of these rocks was accommodated by top-to-the-SW Kerdylion detachment at about 40 Ma (Sokoutis et al., 1993, Brun and Sokoutis 2007, Wuthrich 2009, Kydonakis et al., 2014)

The Eocene extensional event was characterized as the first stage of extension, where the magmatic arc was steady, suggesting that the velocity of the slab retreat was quite slow, at about 1 cm/y (Jolivet and Brun 2010, Philippon et al., 2014, Rocke et al., 2016, Menant et al., 2016). During that time, the HP rocks of the Cycladic Blueschist Unit

were exhumed within the subduction zone (Ring et al., 2010). Soon after, extension migrated to the Cyclades some 35 Ma ago. This second stage of extension was characterized by a fast migration of the magmatic arc, during the southward slab retreat at a high pace (Jolivet and Faccenna 2000, Jolivet and Brun 2010, Jolivet et al., 2015). Simultaneously, another syn-orogenic exhumation process took place in the outer part of the Hellenic arc. The metamorphic rocks of the Phyllites-Quartzites unit (PQ), were exhumed below the syn-orogenic Cretan Detachment in Crete and Peloponnese (Jolivet et al., 2012).

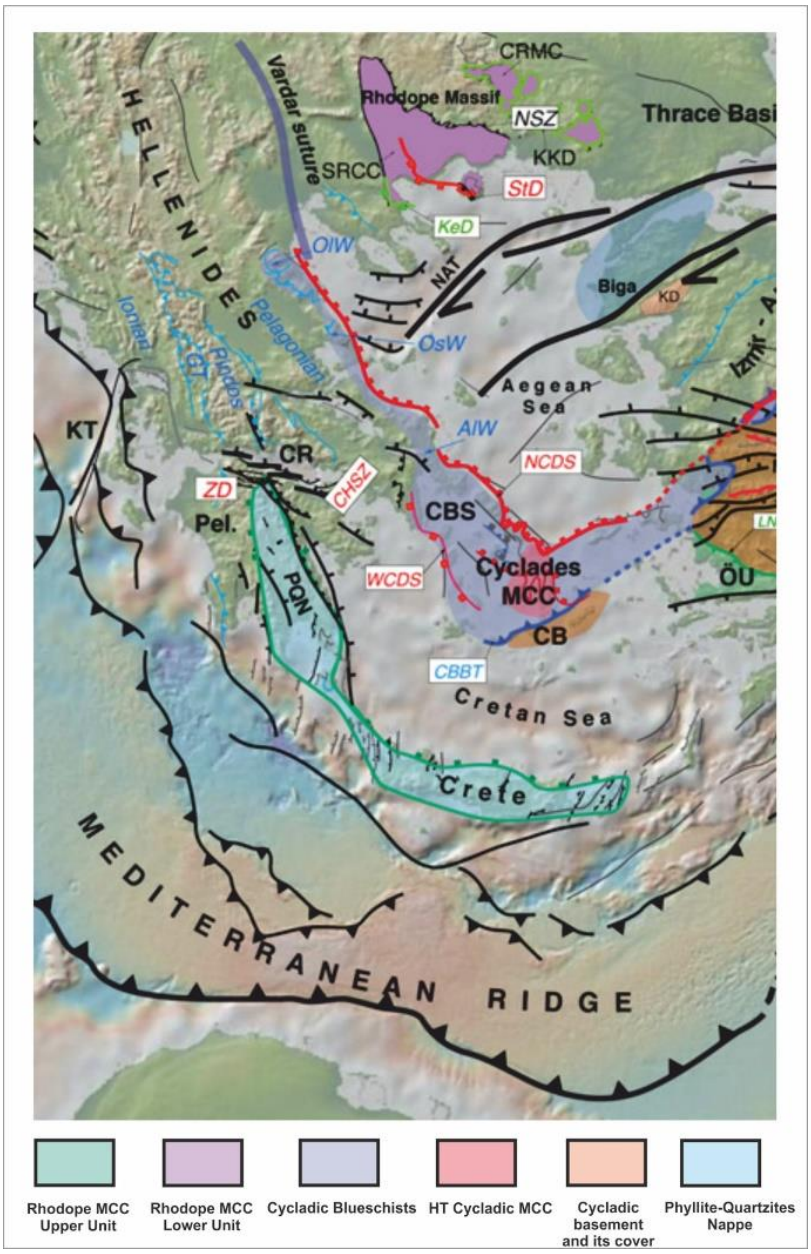

Figure 6: Tectonic map of the Aegean, showing the main lithospheric-scale structures. Active structures are depicted in black lines. The detachment faults in Cyclades and the syn-orogenic detachment faults that were active in Oligo-Miocene time shown in red and light green, respectively (Jolivet et al., 2012).

The N-S extensional episode was followed by an E-W shortening component, which resulted from the southward retreat of the Hellenic trench and the westward escape of Anatolia (Philippon et al., 2014). This shortening event caused:

A) Upright folds with NE-SW to N-S trending axes (Philippon et al., 2014, Menant et al., 2016), e.g., the metamorphic rocks of Tinos, Andros, Naxos (Avigad et al., 2001, Ziv et al., 2010, Philippon et al., 2012) and Paros (Angelier, 1977, Papanikolaou, 1978, 1980, Philippon et al., 2012). B) The local reactivation of the detachment planes as reverse faults (Ring et al., 1999, Avigad et al., 2001, Menant et al., 2013) and C) The separation of the Cyclades in two blocks caused by the development of a dislocation zone the so called Mid- Cycladic Lineament as suggested by Walcott and White (1998), which was interprented as a detachment by Van Hinsbergen and Schmid 2012 or as a dextral strike slip fault of Myrthes-Ikaria by Philippon et al., 2012, 2014. As a result, the northwestern block rotated 22^{o} clockwise and the southeastern block rotated 33^{o} counterclockwise (Morris and Anderson 1996). However, the fact that there are not clear discontinuities, Jolivet et al., 2015 proposed a wide left-lateral gradient of extension induced by the slab tear, which was formed in the eastern Aegean. In addition, the left-lateral displacement of the Aegean does not involve left-lateral faults, but a mantle flowing underneath (fig. 7).

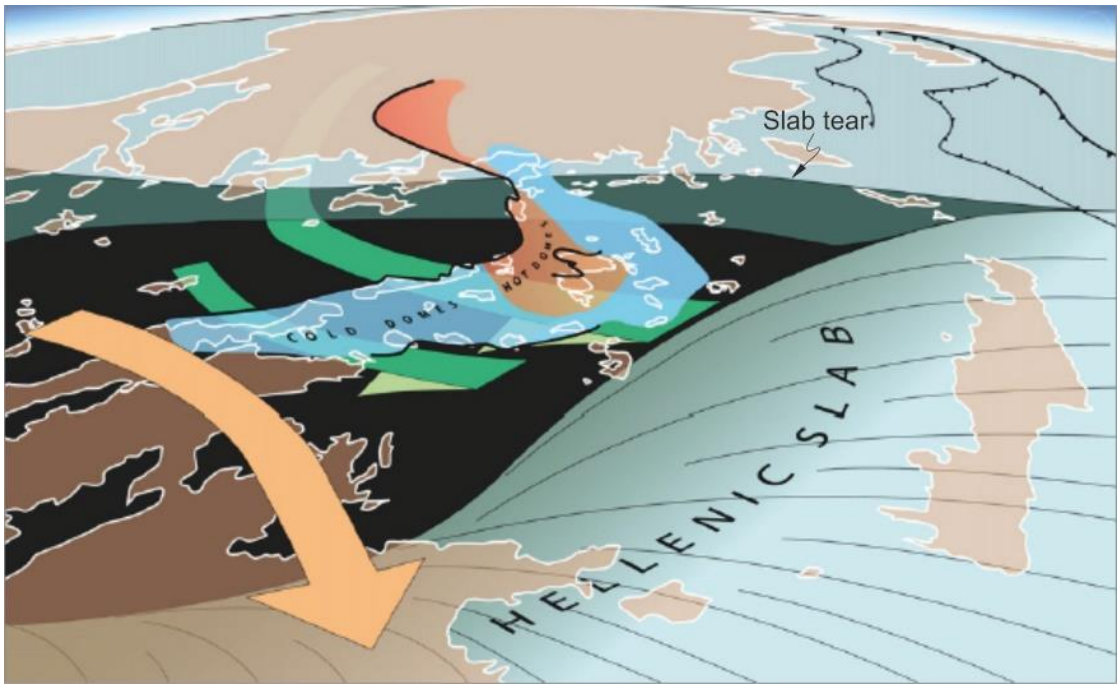

Figure 7: An oblique view on the Aegean, showing the relations between slab tear (black arrow), rotations (light orange arrow) and mantle flow below the Aegean. This mantle flow was triggered by the slab tear and is related to the exhumation of the Ikaria-Mykonos-Paros-Naxos metamorphic core complexes above a hot region (hot domes), in contrast with the other islands that were exhumed in a cold region (cold domes) (modified after Jolivet et al., 2015).

2.4. GEOLOGY OF CYCLADES

The tectonostratigraphy of the Cyclades consists of four tectonic units, which are from top to bottom:

(i) The *Upper Cycladic Unit,* which represents the uppermost unit and is associated to the Pelagonian unit of continental Greece (Durr et al., 1978, Bonneau 1984, Jolivet et al, 2004, Augier et al., 2014). In the Cyclades, rocks of this unit are found as isolated klippen tectonically overlying the Cycladic Blueschist Unit. The Upper Cycladic Unit consists of ophiolitic rocks, (Andros, Tinos, Mykonos, Kea and Serifos) (Melidonis 1980, Jolivet et al., 2010, Grasemann et al., 2012, Augier et al., 2014) or gneisses and schists (Tinos, Syros, Anafi, Donousa) (Durr et al., 1978, Reinecke et al., 1982, Maluski et al., 1987, Patzak et al., 1994, Katzir et al., 1996; Soukis and Stockli 2013). Detrital marine and continental sediments are found in Paros, Naxos, Ikaria Anafi and Mykonos islands (Jansen 1977, Angelier et al., 1978, Papanikolaou 1980, Boger 1983, Sanchez-Gomez et al., 2002, Kuhlemann et al., 2004).

(ii) The dominant unit is the *Cycladic Blueschist Unit* and consists of metabasic rocks interlayered with marbles and metasediments (Papanikolaou 1976, 1977, 1978, Jansen 1977, Augier et al., 2014, Blake et al., 1981, Bonneau et al., 1984, Avigad and Garfunkel 1991, Keiter et al., 2004). Significant outcrops of ultrabasic rocks and metabasites, derived from mid-ocean ridge exposed on Syros island (Augier et al., 2014, Bonneau et al., 1980, Keiter et al., 2004). The Cycladic Blueschist Unit is considered as the metamorphic equivalent of the Pindos unit of continental Greece (Augier et al., 2014, Bonneau et al., 1984, Brocker and Pidgeon 2007, Papanikolaou 1987).

(iii) The *Cycladic Basement Unit*, which comprises Variscan granitoids and orthogneisses mantled by micaschists (Papanikolaou 1977, 1980, Jansen et al., 1977 Durr et al., 1978, Andriessen et al., 1987, Keay 1998, Engel and Reischmann 1998), crops out on the islands of Paros, Naxos, Sikinos Serifos and Ios, and are considered as part of the Apulian platform (Bonneau and Kienast 1982, Keay and Lister 2002). It is worth mentioned that on Naxos and Paros islands the Cycladic basement has undergone a partial melting face in amphibolite to granulite conditions (Jansen and Schuiling 1976, Jansen 1977, Buick 1988, Buick and Holland 1989, Katzir et al., 1999, Duchene et al., 2006, Grasemann et al., 2012).

(iv) The *Basal Unit*, which is part of the External Hellenides, consists of a Triassic to Cenozoic marble sequence overlain by an Eocene metaflysch (Godfriaux 1968; Durr et al., 1978, Dubois and Bignot 1979, Theodoropoulos 1979, Papanikolaou 1979). This unit is tectonically underlying the Cycladic Blueschists Unit in Olympos mt. Evia and Samos islands (Avigad and Garfunkel 1989, Ring et al., 1999).

The rocks of the Cycladic Blueschist Unit were strongly metamorphosed under HP-LT conditions (M1) during Eocene with peak of metamorphism at about 45-50 Ma (Bonneau and Kienast 1982, Bonneau 1984, Wijbrans and McDougall 1988, Buick 1991) at a depth of ~ 50-60 km, and are best preserved today on the islands of Syros,

Sifnos Tinos and Ios. The HP event was followed by a MT-LP overprint (M2) in the Oligo-Miocene times. This overprint is characterized by greenschists facies (Andros, Tinos and Kea), reaching the amphibolite facies and locally partial melting conditions in Naxos, Paros, Ikaria and Mykonos (Jansen 1977, Keay et al., 2001, Huet 2010, Denele et al., 2011, Laurent et al., 2015, Beaudoin et al., 2015).

The exhumation of those HP/LT metamorphic rocks took place in two successive stages: the first stage of syn-orogenic exhumation, occurred in an extrusion wedge as a result of continuous underplating in Eocene time. The best examples for syn-orogenic exhumation are the islands of Evvia, Ios and Syros (Ring et al., 2003, Huet et al., 2009, Jolivet and Brun 2010, Ring et al., 2010, Menant et al., 2016, Roche et al., 2016). The second stage of exhumation took place during Oligocene-Miocene, when CBU rocks where occupying the footwall of low angle normal faults (extensional detachments), associated with top-to-the-NE and top-to-the-SW kinematics (Lister et al., 1984, Jolivet et al., 2010, Jolivet and Brun 2010, Philippon et al., 2011, Grasemann et al., 2012, Soukis and Stockli 2013). This event has led to the development of four main detachment systems in the Aegean region (fig. 8): (i) the North Cycladic Detachment System (NCDS) in the northern part of Cyclades, (ii) the Naxos-Paros Detachment System (N-PDS), (iii) the West Cycladic Detachment System (WCDS) in the western Cycladic islands and (iv) the South Cycladic Detachment System (SCDS), in the southern Cyclades.

(i) North Cycladic Detachment System

In the northern Cyclades, since the first paper, reporting a Cordilleran type metamorphic core complex (Lister et al., 1984), several individual detachments have been described (Faure et al., 1991, Avigad and Garfunkel 1991, Lee and Lister 1992, Gautier and Brun 1994, Ring and Layer 2003, Kumerics et al., 2005, Mehl et al., 2005, Brichau et al., 2007, 2008, Lecomte et al., 2010). Jolivet et al., 2010 suggested that all these structures are part of a single large scale detachment, the so called North Cycladic Detachment System. The NCDS, which crops out on the islands of Andros Tinos and Mykonos , shows a consistent top to the NE sense of shear, and it juxtaposes the CBU in the footwall and the Upper Cycladic Unit in the hanging wall (Faure et al., 1991, Lee and Lister 1992, Gautier and Brun 1994, Ring and Layer 2003, Kumerics et al., 2005, Mehl et al., 2005, Brichau et al., 2007, 2008, Jolivet et al., 2010, Lecomte et al., 2010, Menant et al., 2013). The NCDS is considered as the reactivation of the Vardar ocean suture zone and has exhumed the metamorphic rocks from the Eocene, when it first acted as an normal fault at the top of the extrusion wedge, and then, as a detachment driven by extensional conditions during Oligocene- Miocene (30-9 Ma) (Jolivet et al., 2010, Jolivet et al., 2012).

(ii) Naxos-Paros Detachment System

In the central Cyclades, on the islands Paros and Naxos another large scale low angle normal fault system is formed, which records a top to the N shear sense (Urai et al., 1990, Gautier et al., 1993, Gautier and Brun 1994a, b, Brichau et al 2006, Seward et

al., 2009). The kinematics and structures of the Paros and Naxos extensional system have been described, showing the ductile deformation, which was developed during HT conditions in the lower unit (Gautier et al., 1993), and the transition from ductile to brittle behavior that corresponds to the boundary between the Cycladic Blueschist Unit and the Upper Unit (Brichau et al., 2006). The Naxos-Paros Detachment system was active from 23-5 Ma and accommodated the exhumation of the core complexes in the central Cyclades (Brichau et al 2006, Bargnesi et al., 2013, Menant et al., 2016).

(iii) West Cycladic Detachment System

Studies on the islands of Serifos (Grasemann and Petrakakis 2007, Iglseder et al., 2009, Tschegg and Grasemann 2009, Brichau et al., 2010), Kea (Iglseder et al., 2011) and Kythnos (Grasemann et al., 2012) have documented pervasive S-directed kinematics of low angle normal faults. Grasemann et al., 2012 proposed the existence of a large scale low angle normal fault, which they named the West Cycladic Detachment system (WCDS). Based on thermochronological data, Grasemann et al., 2012 suggested that the WCDS was active during Miocene (~23 Ma) and that a large part of the Aegean extension was accommodated by two bivergent crustal scale detachment systems, the WCDS and the NCDS.

(iv) South Cycladic Detachment System

Several studies have shown evidence for top to the south displacing detachments on the islands of Sifnos, Sikinos (Ring et al., 2001, 2011, Lenauer et al., 2008, Thomson et al., 2009, Brichau et al., 2010) and southern Ios (Lister et al., 1984, Forster and Lister 1999a). Ring et al., 2011 proposed to name these individual detachments, as the South Cycladic Detachment System or South Cycladic Shear Zone (SCSZ), and are preserved at the southern margin of the Cyclades. In addition, the same authors mentioned that this system is considered as the southern termination of the WCDS. However, Augier et al., 2014 reported that on the island of Sikinos the development of the top to the south kinematics predates the top to the north structures. Just as on Sikinos island, the same kinematics were observed on southern Ios (Huet et al., 2009), where the SCSZ is observed at the base of CBU and was first interpreted as an extensional shear zone by Lister et al., 1984 and then reinterpreted as a thrust (Huet et al., 2009). Menant et al., 2016, mentioned that the SCSZ is considered as the base of the extrusion wedge during the syn-orogenic exhumation of the HP rocks of the CBU (Ios), and at the top was bounded by the Vari detachment (Syros).

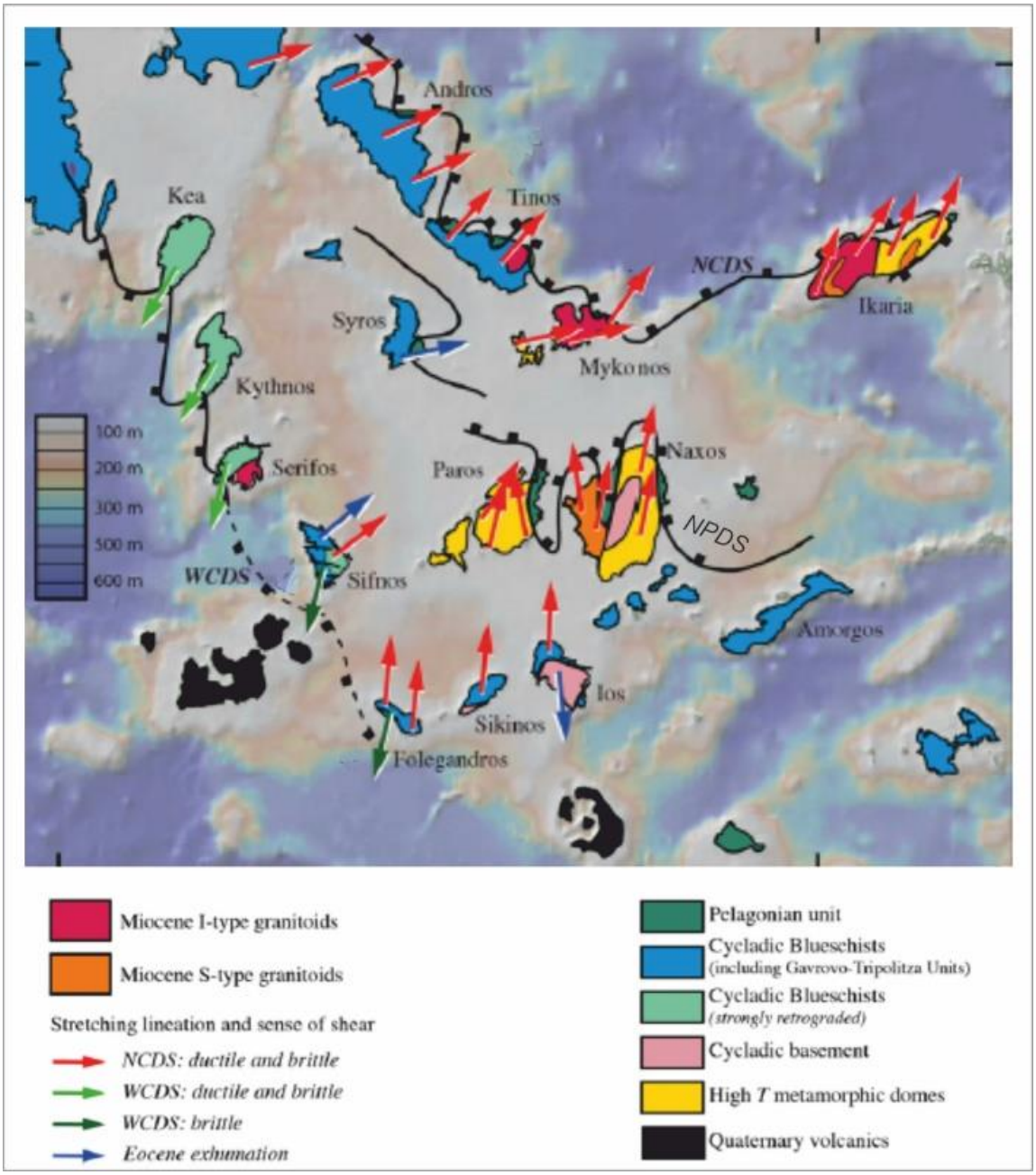

Figure 8: Tectonic map of the Cyclades, showing the main tectonic units and the crustal-scale detachment systems. Arrows represent the sense of shear in the area. The western Cycladic area shows a symmetrical pattern of extension, in contrast with the central Cycladic area, where an asymmetric pattern with top-to-the-north shearing is recorded in most islands (Jolivet et al., 2015, Gautier and Brun 1994a,b, Huet et al., 2009, Jolivet et al., 2010, 2013, Grasemann et al., 2012, Augier et al., 2015).

3. GEOLOGY OF HERAKLIA

3.1. LITHOLOGY

Heraklia is located at the center of Attic-Cycladic metamorphic core complex between the two metamorphic domes of Naxos and Ios, both of which were exhumed below low-angle detachment faults (fig. 9, Jolivet et al 2010).

The metamorphic succession of Heraklia belongs to the Cycladic Blueschist Unit (CBU). Previous studies on the island, were carried out by Seckel 2004, Behrmann and Seckel 2007, who reported that Heraklia is dominated by a thick sequence of variegated and white calcite marbles interleaved with mega- boudins of dolomitic marbles. The same authors mentioned that metapelitic schists intercalated with marbles are exposed on the central and southwest part of the island. Additionally, numerous metabauxites and laterites are preserved at the top of the thick sequence of the variegated marbles in the northwest part of the island (Behrmann and Seckel 2007, Brodhag et al., 2003).

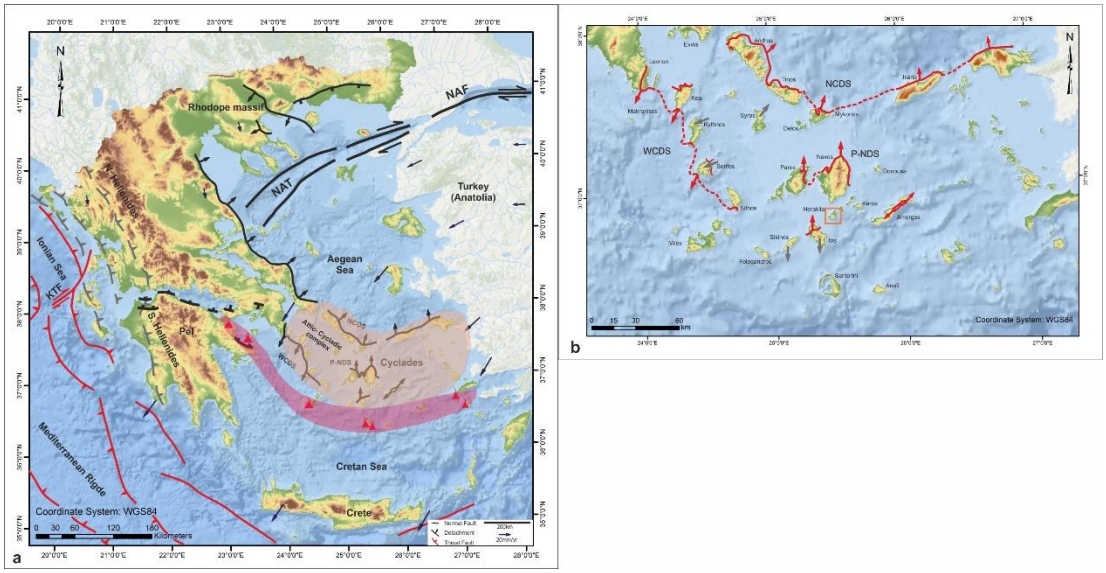

Figure 9: a) Tectonic map of Aegean illustrating the main structures and the location of the Attic-Cycladic metamorphic core complex within the Hellenic orogen. b) Location of Heraklia Island within the Attic- Cycladic complex (North Cycladic Detachment System (NCDS), Paros-Naxos Detachment System (P-NDS) West Cycladic Detachment System (WCDS)) (compiled from Avigad and Garfunkel, 1991; Gautier and Brun, 1994; Huet et al., 2009, Jolivet et al., 2010, Lekkas et al., 2011, Grasemann et al., 2012, Ring et al., 2010, Soukis and Papanikoaou 2004).

An extensive study was carried out on Heraklia Island, which included detailed mapping in 1:10.000 scale (fig. 9). The main lithologies of Heraklia island from bottom to top are: a) quartz-mica schists interlayered with lenses of orthogneissic bodies, b) white ultramylonitic marbles overlain by a thick sequence of coarse-grain variegated marbles, c) quartz-mica schists intercalated with thin bedded marbles (fig. 10) and d) Neogene sediments, which comprise mainly sandstones with cross-bedded layers and conglomerates (fig. 11).

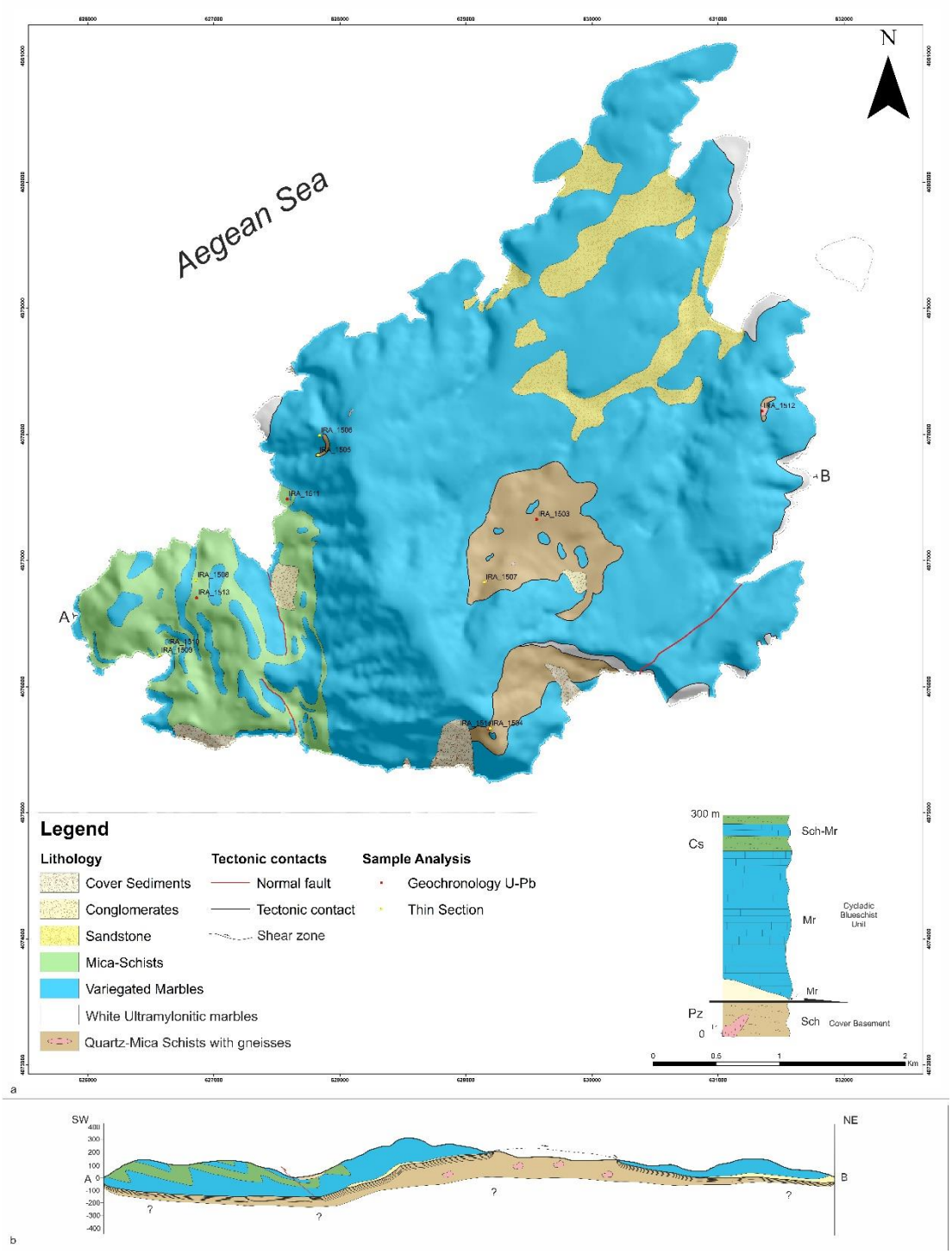

Figure 9: a. Detailed geological map of Heraklia Island at 1:10,000 scale and cross-section (b), showing also sample location collected for U-Pb detrital zircon dating (red circles) and thin-section analyses (yellow circles).

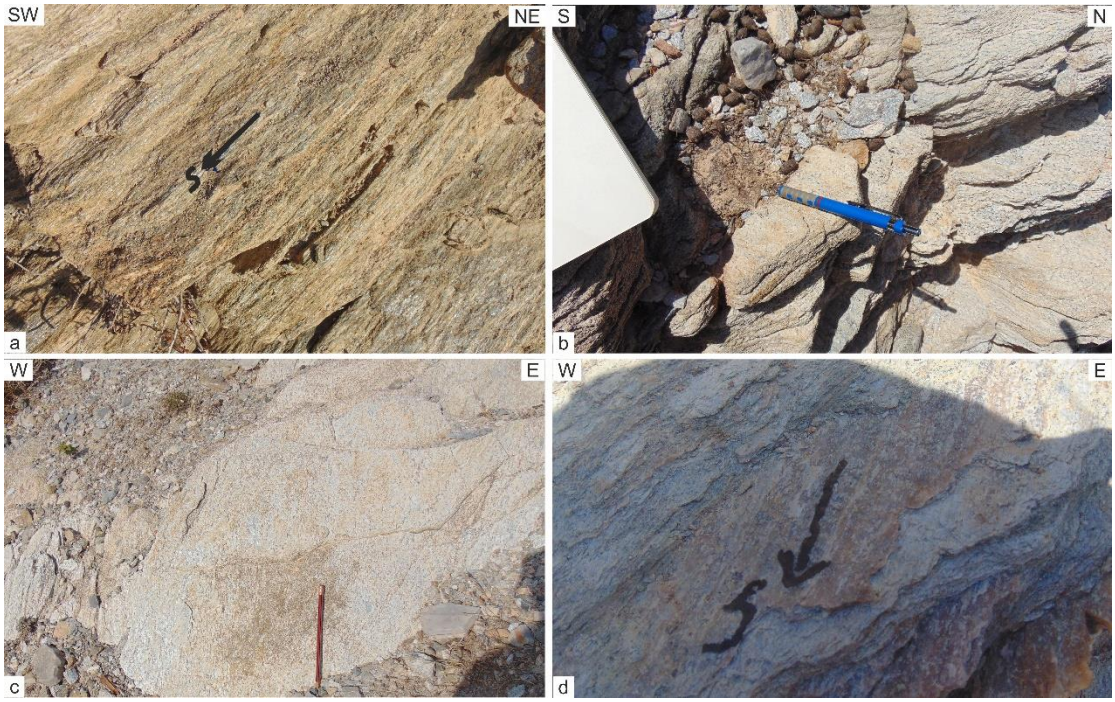

Figure 10: a. Lowermost mylonitic quartz-mica-schists from the central part with N-S stretching lineation, b, c. Strongly foliated orthogneissic rocks, observed within the lowermost schist sequence and d. Uppermost quartz-mica-schists from the southwestern part of the island. In all photos black arrows indicate the N-S stretching lineation.

Figure 11: a. Outcrop of conglomerates from the central part of the island and b. Sandstones that are exposed on the northern part of Heraklia.

The uppermost quartz-mica schists and the variegated marbles are crop out at the western and southwestern part of the island. The contact between these two lithologies, shows evidence of transition that appears to be folded by large scale N-S isoclinal folds. On the other hand, the marbles and the lowermost quartz-mica schists with the orthogneissic bodies are observed at the central part of the island and, a mylonitic foliation is developed along the contact between these underlying quartz-mica-schists and the overlying marbles (fig. 12). Additionally, white ultramylonitic marbles are exposed around the island below the main thick sequence, but they are not observed at the central part of the island (fig. 13). Finally, the rocks of the CBU are unconformably covered by sedimentary rocks, which comprise sandstones and conglomerates that crop out on the northern, southwestern and central part of the island. The age of the sandstones appears to be late Miocene, based on a group of Miogypsina sp. foraminifera that was found in these sediments (Behrmann 2007, Seckel 2004) and the conglomerates are derived from the erosion of the CBU lithologies.

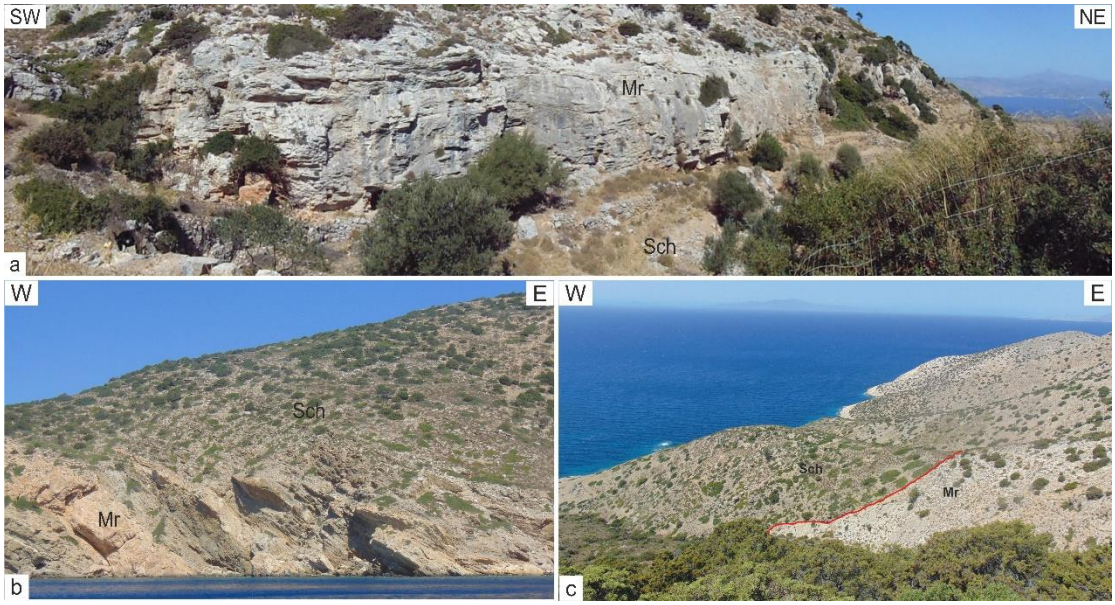

Figure 12: a. Main tectonic contact between the lowermost schists and the marbles from the central part of the island, b. View of the uppermost schists intercalated with thin bedded marbles from the southwestern part of Heraklia and c. North of Vourkaria Bay, where the quartz-mica- schists are overlying the marbles (red line) in the SW part of the island.

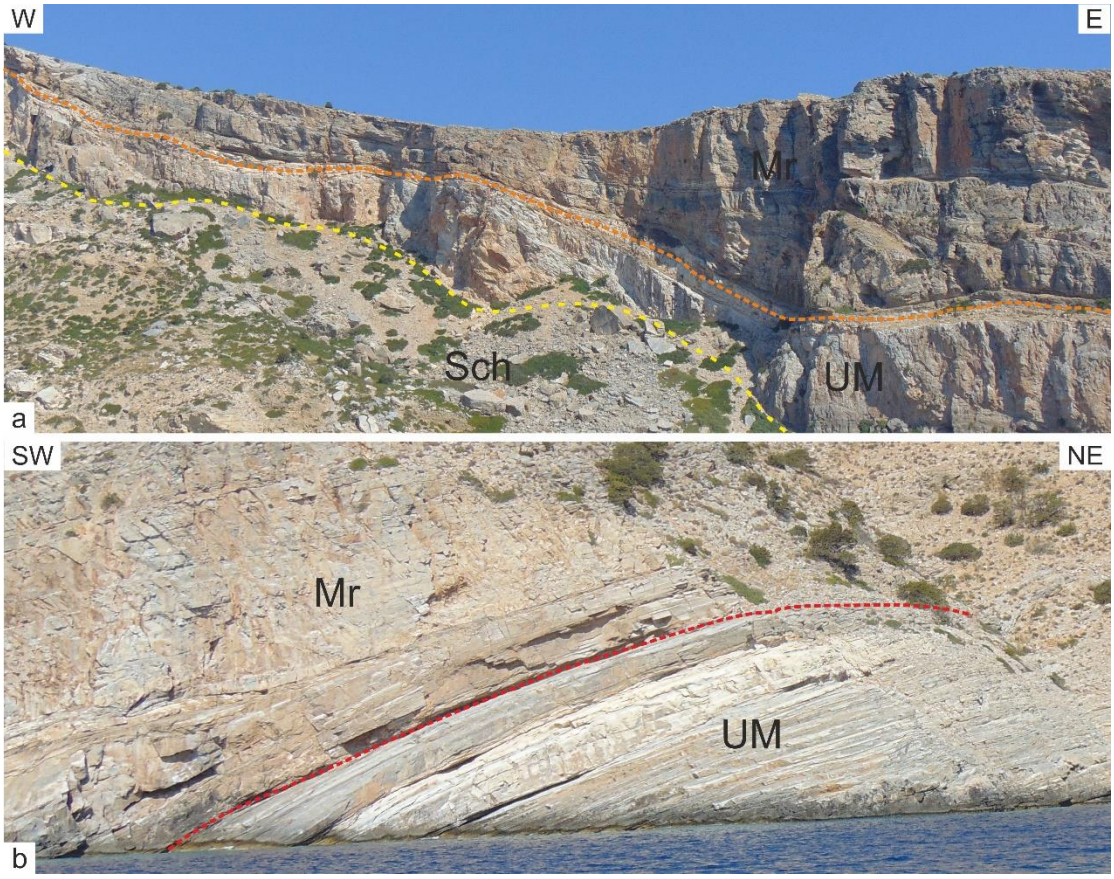

Figure 13: a. Southern part of the island, where the quartz-mica schists are observed below the ultramylonitic marbles (yellow line) and the variegated marbles (light orange line), and b. View of the contact (red line) between the underlying ultramylonitic marbles (UM) and the overlying variegated marbles (Mr).

3.2. STRUCTURES

The rocks of the CBU include structures, which are related to the retrograde path, and developed under greenschists facies conditions, during exhumation processes (D2). These structures are related to a mylonitic foliation associated with a stretching lineation, and isoclinal folding. Previous structures, related to the prograde path (D1) and an earlier metamorphic event, are not recorded on Heraklia Island, due to strong greenschists overprint. However, just as on SE Naxos island, relics of the HP event are only preserved in the form of inclusions.

DUCTILE DEFORMATION

Macroscopic observations on the rocks of CBU on Heraklia island, revealed that the oldest penetrative foliation (S2) has been developed under greenschists facies during the first stage of deformation (D2), forming axial plane isoclinal folds. Additionally, a stretching lineation (L2) has been developed, which is characterized by mineral assemblages, such as chlorite, K-feldspar, quartz and micas. Measurements of penetrative foliation and stretching lineation were obtained from all lithologies and are presented in stereo-plots in Figure 14. Foliation planes dip variably at shallow angles. Stretching lineations, which are formed on these foliation surfaces, are oriented in NNW-SSE to N-S direction.

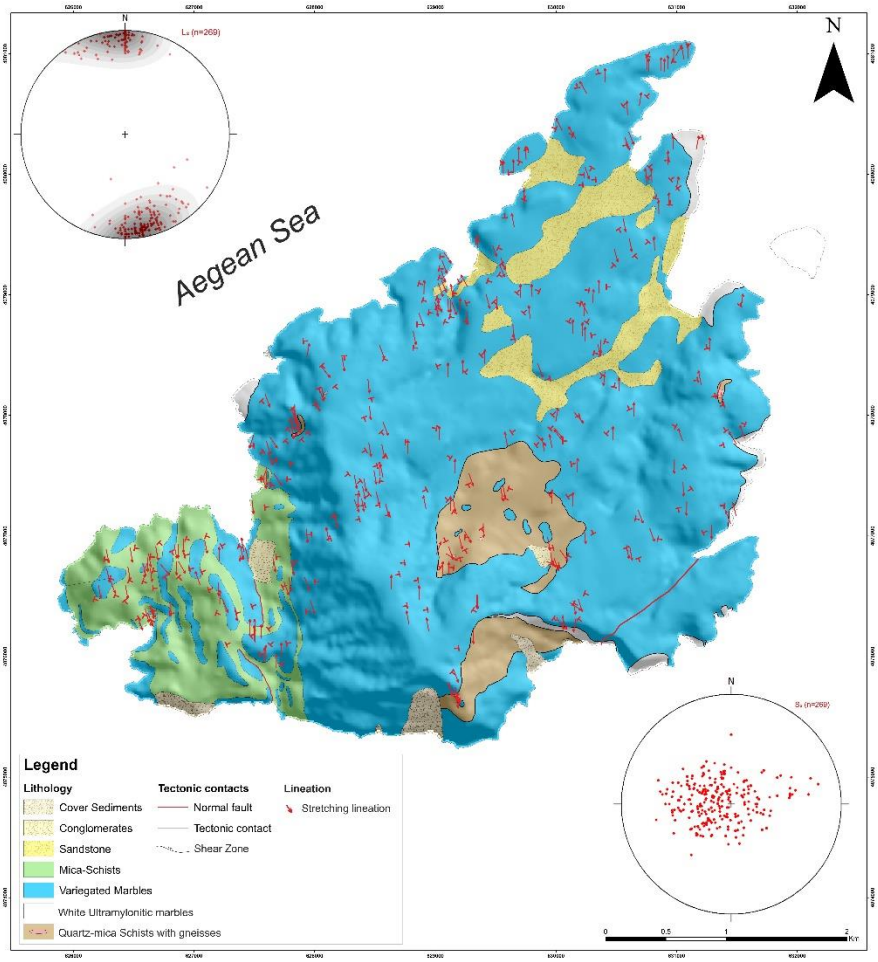

Figure 14: Tectonic map of Heraklia Island, with stretching lineations (L2), which developed during the main phase of deformation (D2). Poles to (S2) foliation, associated with stretching lineation (L2) are presented in stereoplot (lower hemisphere equal-area projection).

However, there is evidence for an older foliation (S1), related to the Eocene HP metamorphic event (D1), as glaucophane is observed in the form of inclusions in albite porphyroblasts syn-tectonic to the retrograde greenschists facies assemblages (fig. 15). Subsequently, the S2 foliation has been intensely deformed with isoclinal folding. These isoclinal folds are observed on the marbles, folding the S2 foliation and forming an axial plane cleavage (S3) and a N-S intersection/stretching lineation (L3) (fig. 16).

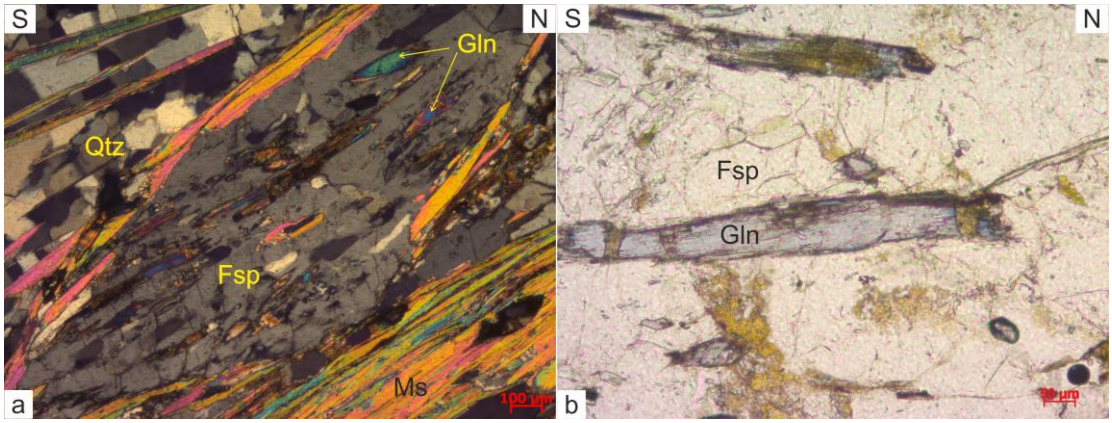

Figure 15: Photographs of thin sections from the quartz-mica schists, of the SW part of the island. (a). Feldspar porphyroblast with the presence of glaucoplane in crossed polars, and (b). Elongate glaucophane grains boudinaged during D2.

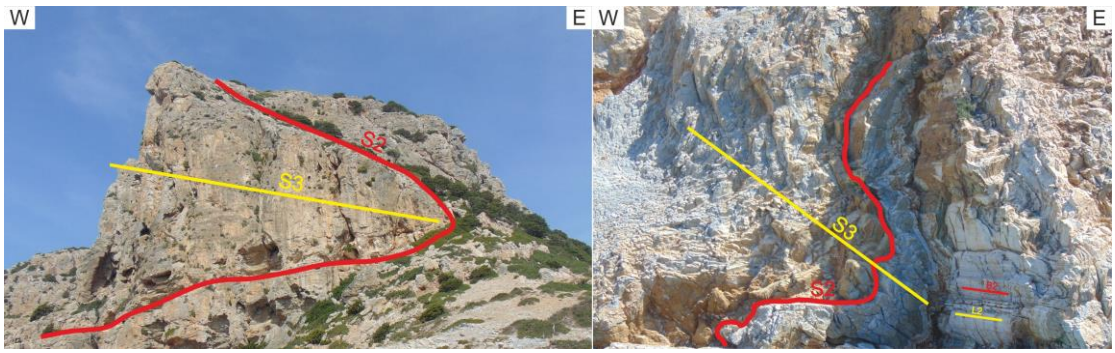

Figure 16: a. Large-scale S2 isoclinal fold trending N-S and b. Axial plane cleavage (S3) and a N-S intersection/stretching lineation parallel to the B2 fold axes (southern part of the island).

S-C' fabrics are developed in the lowermost and uppermost schists of the CBU, revealing an overall top-to-the-north sense of shear. In the central part of the island, the shear zone shows a brittle- ductile fabric, and is characterized by numerous kinematics, all of which display a top-to-the-north shearing. The intensity of the shear bands, which are observed in the lowermost schist unit, are drastically decreased near the contact with the overlying marbles, and in some cases, they are overprinted by cataclastites (fig. 17). In addition, the orthogneissic rocks reveal the same overall top-to-the-north kinematics. In contrast with observations in the outcrop scale, in thin sections, both schists and orthogneisses develop unambiguous S-C' type shear bands that indicate top-to-the-north shearing, but top-to-the-south shear bands are sparsely

observed. In more details, the orthogneisses (samples IRA_1507 and IRA_1504), which are exposed on the central and southern part of the island within the quartz-mica schists, consist of garnet, quartz, muscovite, albite and chlorite. The garnets occur as porphyroblasts, which are stretched and rotated towards the south (fig 18).

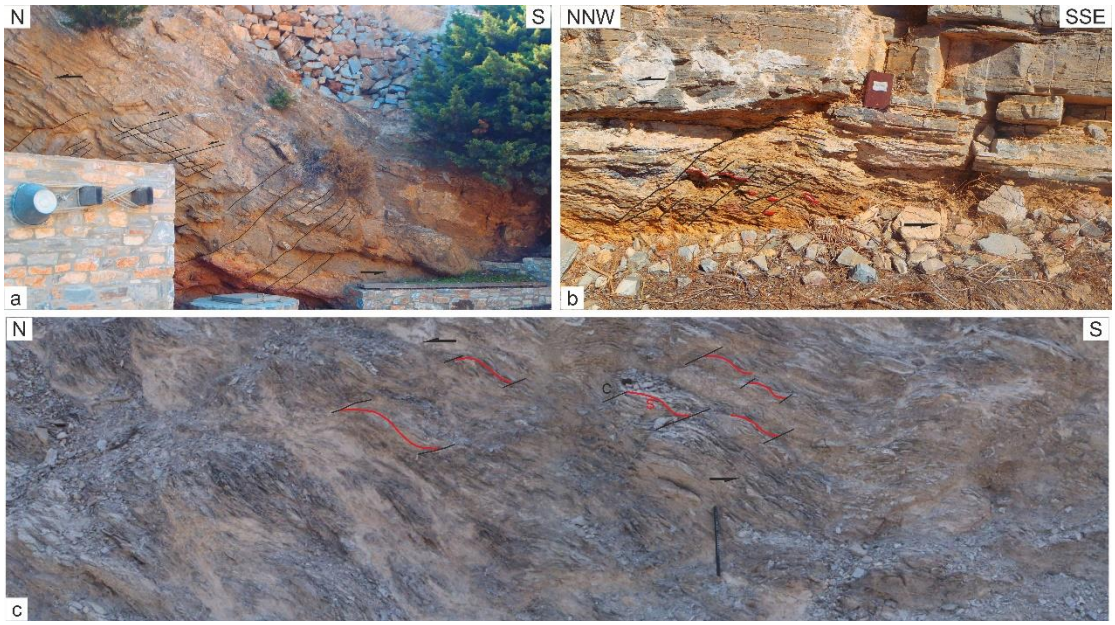

Figure 17: Kinematic indicators observed in the lowermost schist unit from the central part of the island. a and b. Top-to-the-north kinematic indicators (sheared lenses of quartz and normal micro-faults), c. S-C' shear bands, which are developed in the quartz-mica-schists. All kinematic indicators display a consistent top-to-the-north sense of shear.

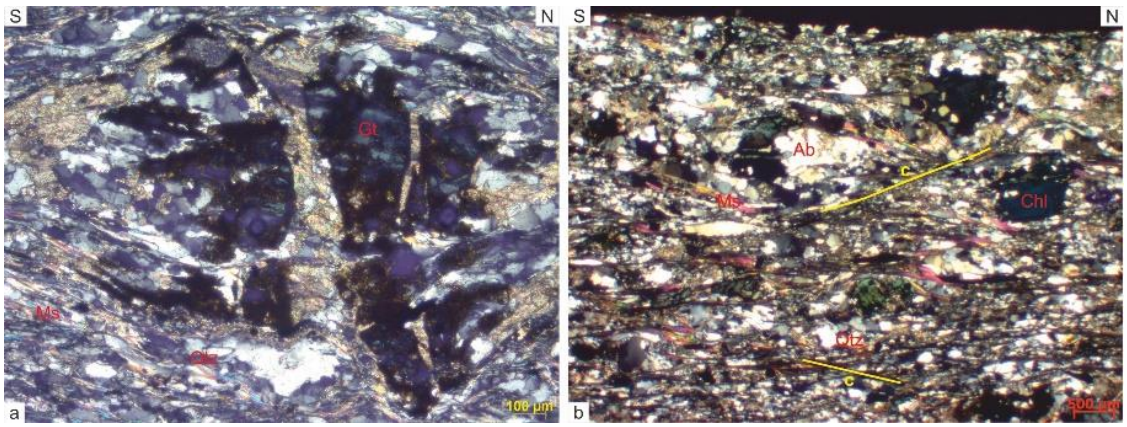

Figure 18: Thin sections (crossed-polars), parallel to stretching lineation. a. Stretched and rotated (to the south) garnet from the orthogneissic rocks (sample IRA_1504) and b. Top-to-the-north and south shear bands in the orthogneiss, which crop out on the southern part of the island (sample IRA_1507).

Generally, the main foliation of the quartz-mica schists is mostly composed of greenschist-facies minerals, such as feldspar, muscovite, chlorite, quartz and occasionally garnet. Feldspar appears in the form of syn-tectonic porphyroblasts in which very often inclusions were observed. These inclusions are in many cases syn-greenschists-facies minerals but in some occasions the presence of relic glaucophane

grains can be observed. They represent evidence for the earlier HP-metamorphic event. Recrystallized quartz and micas characterize the matrix of all samples. Isolated syn-tectonic and post-tectonic garnet porphyroblasts are observed. Kinematic indicators from all samples mostly display both top-to-the-north, but top-to-the-south shearing is also observed (fig. 19).

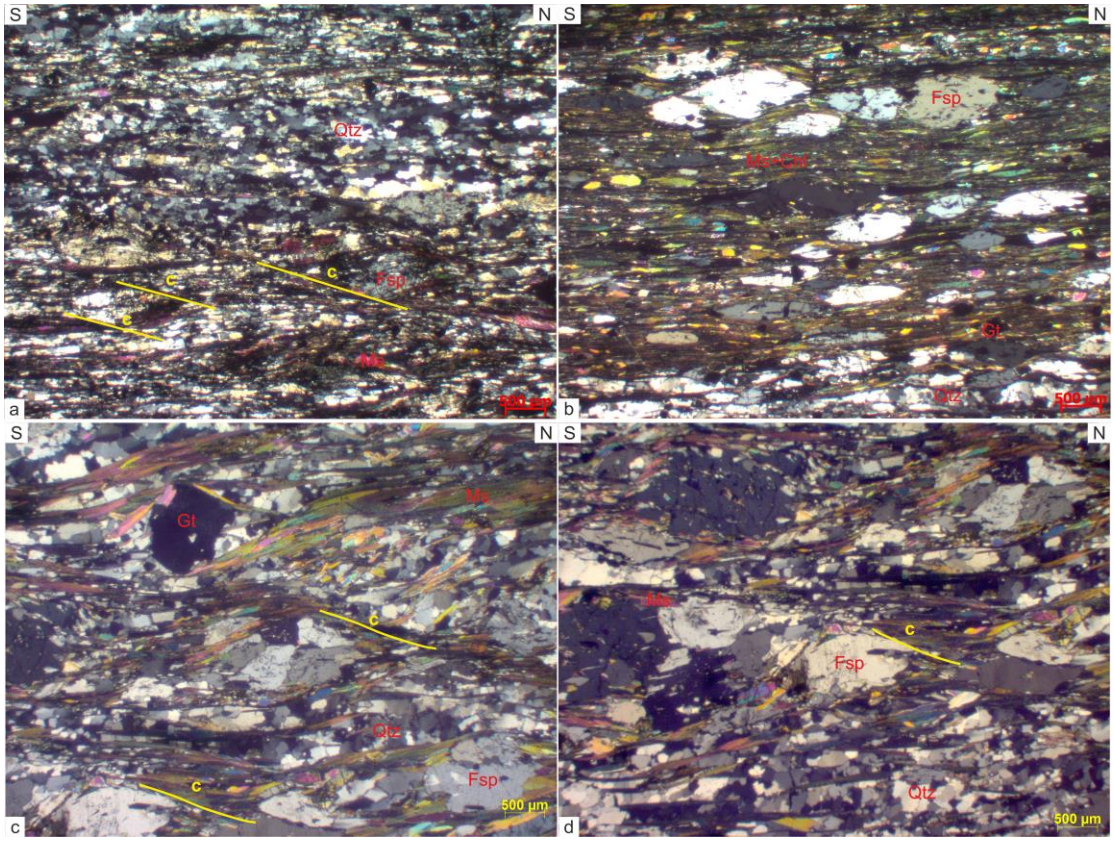

Figure 19: Thin sections (crossed polars) of mylonitic foliations. a. Sample IRA_1510 consisting mostly of quartz and less muscovite, the main foliation is cut by the C' shear bands, b. Sample IRA_1509, which includes feldspar, quartz, muscovite, chlorite and garnet. The overgrown syn-tectonic feldspar porphyroblasts is bounded by muscovite and chlorite. Small post-tectonic garnets are observed as well. c and d. Sample IRA_1508, which consists of syn-tectonic feldspar and garnet porphyroblast. All samples show characteristic S-C shear bands, indicating mostly top-to-the-north sense of shear.

Thin section from the marbles reveal kinematic indicators such as δ-type porphyroclast, indicating top-to-the-north sense of shear similar to the non-mylonitic parts of the sequence (fig. 20).

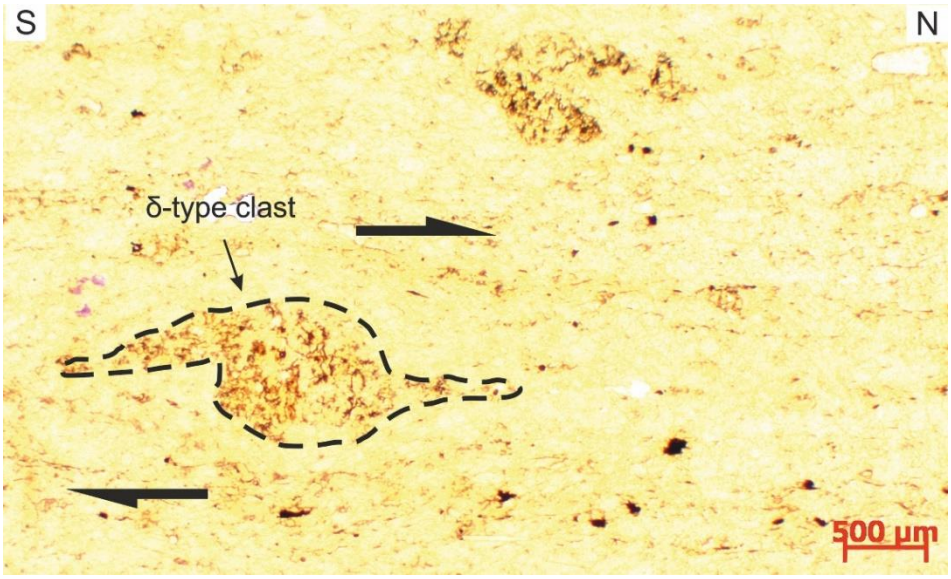

Figure 20: a. Microphotograph of the ultramylonitic foliation in the marbles with a δ-type porphyroclast.

Finally, contemporaneous with the top-to-the-north shearing deformation, eye-folds are developed in the ultramylonitic marbles with an overall N-S trending axis, which are observed at the southern part of the island (fig. 21).

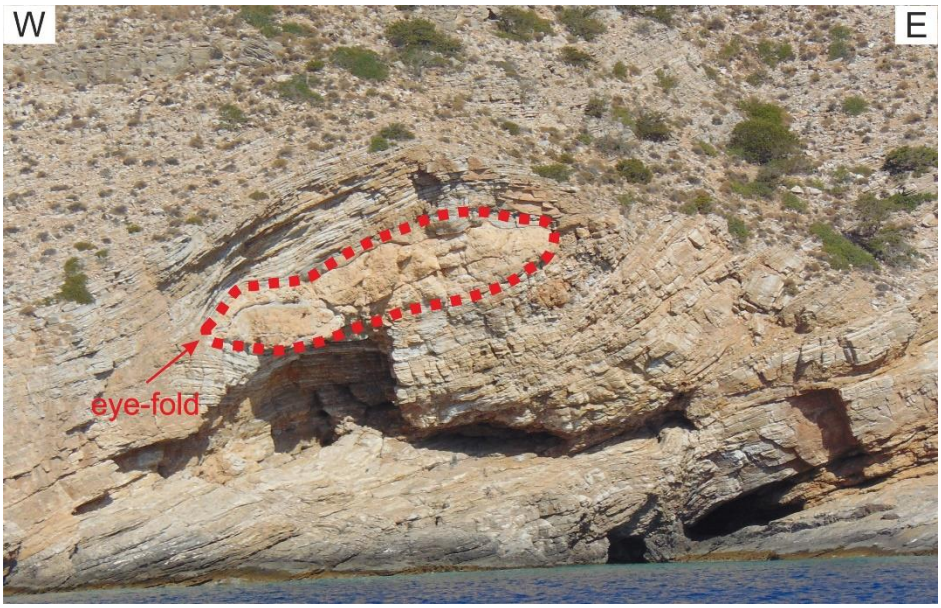

Figure 21: Eye fold in the ultramylonitic marbles from the southern part of Heraklia island.

BRITTLE DEFORMATION

In Heraklia the final stage of deformation includes structures that are related to NW-SE and NE-SW normal faulting. The SW part of Heraklia is controlled by the Vourkaria most probably normal fault, which trends NW-SE and dips towards to the northeast. This fault cuts the contact between the marbles and the quartz-mica schists, and is generally sub-parallel to the regional foliation. In addition, a fault breccia has been developed on the Vourkaria fault's plane, as a result of its activity. Another fault is observed at the southestern part of the island, which trends NE-SW and dips towards to the northwest. Close to the fault plane a characteristic drag zone has been developed that indicate its normal activity. Finally, small-scale-normal faults are developed in the marbles, all over the island (fig. 22).

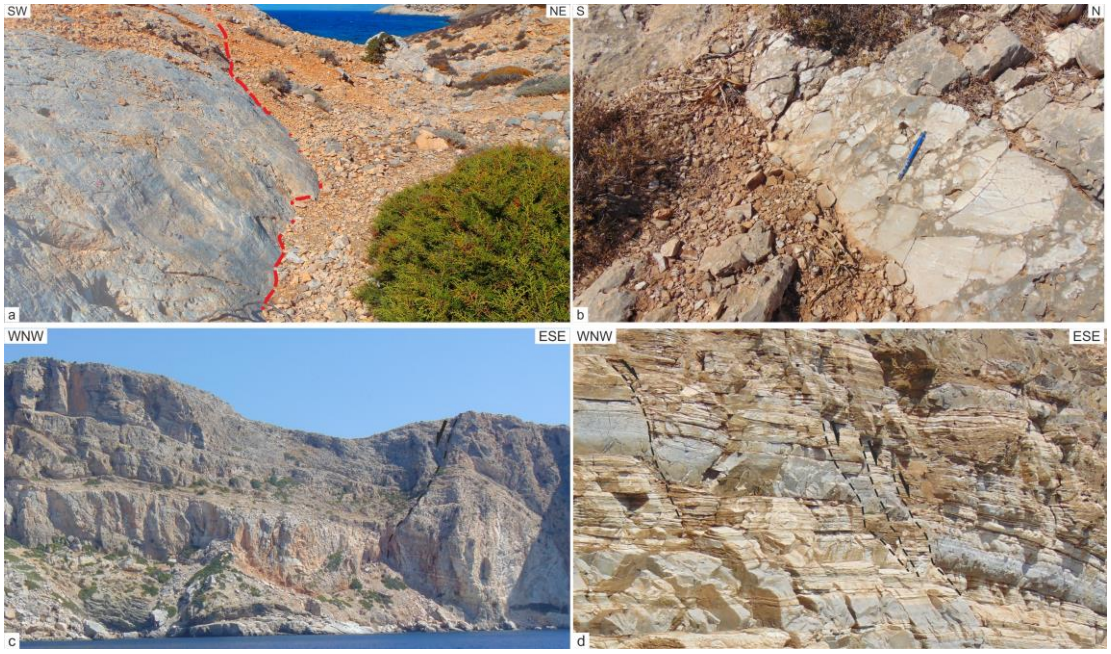

Figure 22: a. The Vourkaria normal fault in the SW part of the island, trending NW-SE and dips towards to the northeast, b. Fault breccia from the southwestern part of the island trending NW-SE, c. The high-angle Meriha normal fault, and d. Outcrop of normal small-scale faults in the marbles, from the southern part of the island, trending NNE-SSW.

4. U-Pb Detrital Zircon Dating

4.1. Analytical Method

U-Pb (Uranium- Lead) chemical geochronology is one of the oldest and important isotopic dating methods, capable of measuring events from the early solar system ~ 4.57 Ga into the Pleistocene (Schoene 2014, Barrell 1917, Bateman 1910, Boltood 1907, Holmes and Lawson 1927). The element lead has four stable isotope, ^{204}Pb, ^{206}Pb, ^{207}Pb, and ^{208}Pb, of which the latter three have a radiometric component produced through the independent decay of ^{238}U, ^{235}U and ^{232}Th respectively. The abundance of high-U minerals in most rock types, and the resistance of many of these minerals to chemical- physical weathering, contributes to the popularity of the U-Pb system. U-Pb dating is most commonly performed on the mineral of zircon, though it can be used on other minerals, such as monazite, apatite, xenotime, titanite, rutile, baddeleyite, allanite and pervoskite (Schoene, 2014 and references therein).

In this study, U-Pb detrital zircon dating was carried out from five metamorphic rocks (schists and orthogneisses) from the island of Heraklia, using a laser ablation-inductively coupled plasma-mass spectrometry (LA-ICP-MS) at University of Texas at Austin, Jackson School of Geosciences, Department of Geological Sciences UTChron Laboratory.

In order to perform the geochronology procedure separates of zircons were required. The first stages of this procedure demanded crushing of the rock samples. These separates were washed in order to remove the dust or clay size particles, and the heavy ones were dried at room temperatures (25^{o} C) and used for the next stages. Then, the heavies were separated further using heavy liquid (Bromoform Geoliquid), and passed through the Franz magnetic separator in order to remove mafic grains, such as micas. Franz magnetic was followed by another heavy liquid separation (MI-GEE Methylene Iodide) so that the zircons were separated from the remaining minerals.

Moreover, zircons were mounted under the microscope and located onto 1-inch double sided polycarbonate rounds. An Analyte G2 193 nm ArF excimer laser equided with a two-volume, large format HELEX cell was used, in order to ablate thirty spots on each zircon grain. Supremely fast washout times (<0.3s) come of the use of HELEX cell. A thermoFisher Element II single collector, magnetic sector, HR-ICP-MS was used so that U, Pb isotopes could be measured on.

At least 120 zircons were generally analyzed unpolished per sample, using the laser perpendicular to the c-axis of the grain's prism surface (Vermeesch 2004). Discrete age for each grain was assessed on the Concordia diagram (Wetherill 1956). This procedure yielded the best age for each zircon with an error at the 2σ level. The Visual Age data reduction scheme was used so that the data could be reduced (Petrus and Kamber, 2012). Thus, according to the $^{206}Pb/^{238}U$ and $^{207}Pb/^{235}U$ age, the age integrations that were less than 1 Ga and more than 10% discordant, were excluded.

The analytical data and calculated ages of all samples from Heraklia are listed in Table 2 (see appendix).

4.2. U-Pb Results

Two samples from the uppermost schist unit, which crop out on the western and southwestern part of Heraklia, and one sample from the lowermost unit from central part of the island, were collected for U-Pb dating in order to obtain the age of detrital zircons. The zoned zircon grains were targeted in order to ensure measurement of the rim and core ages. The youngest populations of core ages are considered as the maximum depositional age of the rock, whereas the rim ages correspond to metamorphic events.

At about 120 zircons were picked up, for analysis from each sample. The core of zircons from samples *IRA_1511* and *IRA_1513* from the western and southwestern of Heraklia respectively, yielded maximum depositional ages at about 80 Ma (Late Cretaceous) and they have a metamorphic rim age at ~50 Ma (Eocene). Even though these two samples share many similarities, there are some differences in zircon populations. The sample *IRA_1511*, for instance, has a core age in Jurassic, Devonian and Ordovician, whereas the sample *IRA_1513*, has a core in Silurian. The zircons from the lowermost schists (sample *IRA_1503*), yielded Paleozoic ages (~550 Ma). As can be seen on the diagram, these schists did not yield younger ages than 500 Ma. Finally, two samples from the orthogneissic rocks were analyzed as well. These orthogneisses crop out on the southern (*IRA_1514*) and northeastern (*IRA_1512*) part of the island and they are considered as lenses within the quartz-mica schists. The best depositional age for these rocks was estimated approximately at 230 Ma, as a maximum core age in Triassic is well-represented. Just as on the quartz-mica schists, there are differences in core ages. The sample *IRA_1512* has a core age in Carboniferous (~310 Ma), whereas, the sample (sample *IRA_1514*) has a core age of 440 Ma (fig. 23, table 1).

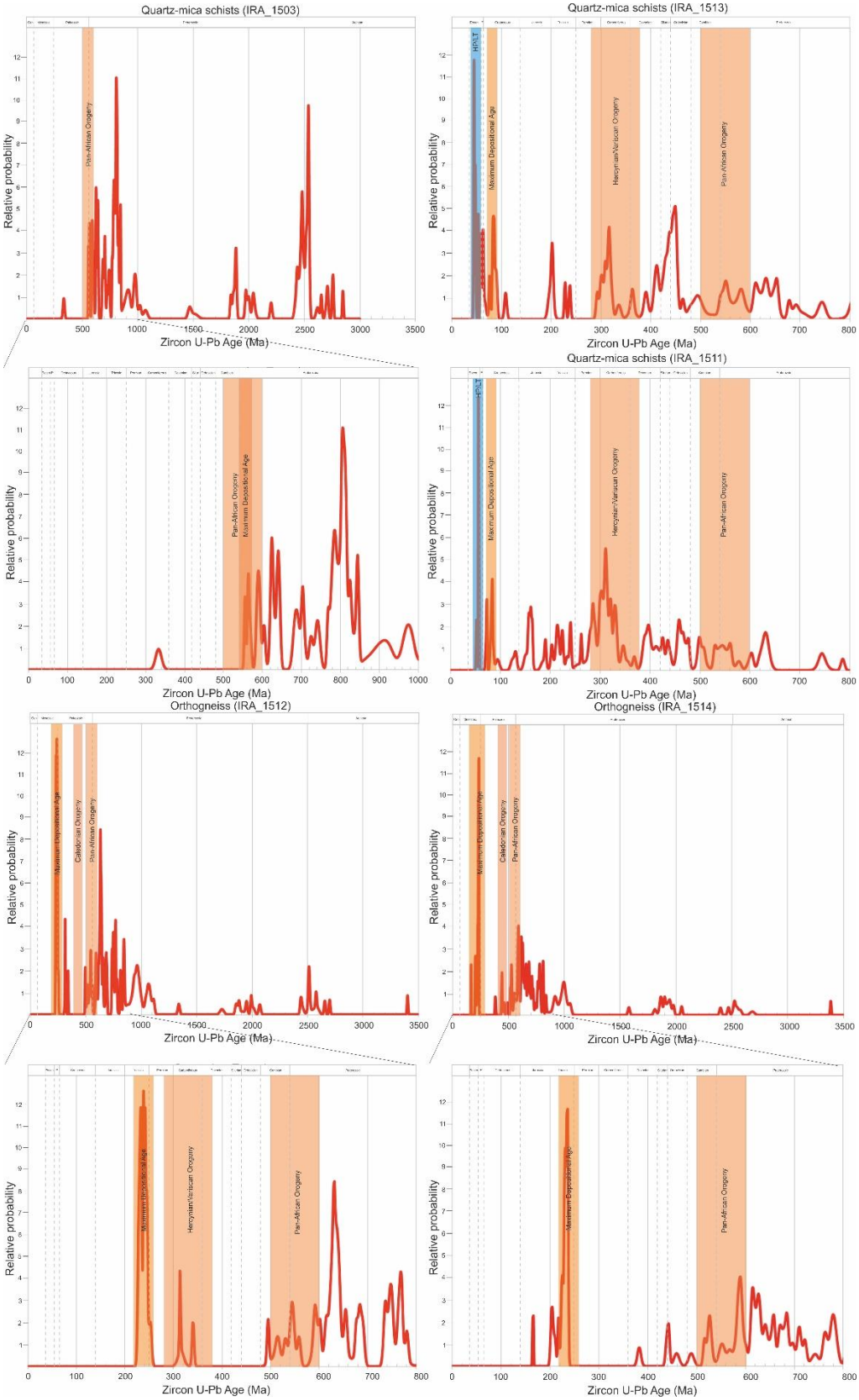

Figure 23: U-Pb geochronology results. The diagrams show the compiled data from 3.500-0 Ma. The diagrams, which show the compile data from 800-0 Ma, are the expanded portions of the original ones. Maximum depositional ages are depicted in orange, metamorphic events and orogenic events, through geological time are depicted in blue and red, respectively.

Table 1: Location of the samples that were used for U-Pb geochronology.

Sample	Unit	Latitude	Longitude	Lithology
IRA_1503	CB	36.83554 N	025.45464 E	quartz-mica schists
IRA_1511	CBU	36.83726 N	025.43249 E	quartz-mica schists
IRA_1512	CBU	36.84303 N	025.47485 E	gneiss
IRA_1513	CBU	36.83029 N	025.42430 E	gneiss
IRA_1514	CBU	36.82063 N	025.45015 E	quartz-mica schists

5. DISCUSSION

5.1. LITHOLOGICAL UNITS OF HERAKLIA ISLAND

Previous works in Heraklia island has been carried out by Avdis and Triantaphyllis 1994, who produced the first geological map of Heraklia island, and Berhmann and Seckel 2007, who studied the deformation history and estimated flow stresses in the metamorphic rocks of the island. These authors have distinguished two main lithological units probably of Triassic age. The lowermost lithological unit, which consists of metapelitic schists and marbles, and are exposed at the central and southwestern part of the island, and the uppermost lithological unit, which compises a thick sequence of variegated marbles with white calcite and dolomite marbles. Even though, the lithologies of Heraklia island have been studied and mapped in detail, the nature of their contacts have not been described yet, leaving some questions concerning the relations between these lithologies unknown. According to our new field observations and detailed mapping at 1:5000 scale, three lithological units were identified on the island of Heraklia:

1. The structurally lowermost lithological unit crops out at the central and southern part of the island and consists of light brown quartz mica schists with minor lenses of fine-grain orthogneissic rocks. The initial contact between the orthogneisses and its country rock could not be determined due to intense deformation.
2. The intermediate lithological unit is composed of a thick sequence of coarse grain variegated marbles, which represent the main body of Heraklia. At the base of these marbles, white ultramylonitic marbles showing localized ductile deformation are observed, and are only exposed around the island. In addition, at the top of the lowermost quartz mica schist unit the presence of numerous shear bands indicate that the contact between the aforementioned units is defined by the development of a shear zone, displaying an overall top to the north shearing.
3. The uppermost lithological unit comprises light brown to light green quartz mica schists with thin-bedded marbles, and crop out at the western and southwestern part of the island. These schists are in contact with the variegated marbles, and the nature of this contact shows a clear transition, though it appears to be folded with a N-S fold axis. These schists with abundant micas and less quartz-feldspar aggregates than the lowermost schists, contain relics of glaucophane, which show evidence for an earlier HP-LT metamorphic history and it links these rocks to the Cycladic Blueschist Unit.

5.2. STRUCTURAL ANALYSIS

According to structural analysis the main foliation Sn has been developed under greenschist facies conditions, and a NW-SE to N-S stretching lineation has been formed on these foliation planes. Evidence for an older foliation Sn-1 associated with a stretching lineation Ln-1 is only observed in thin sections from the uppermost schists. During the main phase of deformation, the main foliation Sn has been isoclinally folded with a N-S fold axis, which resulted in the development of a cleavage

Sn+1 and a stretching/intersection lineation Ln+1 parallel to the fold axis. In addition, a mylonitic foliation is observed on the white ultramylonitic marbles and at the upper part of the lowermost quartz mica schists. Shearing during the main phase of deformation took place along the contact between the lowermost and intermediate units, and it was top to the north. We name this contact the Heraklia shear zone and we suggest that it is probably linked to the Paros Naxos Detachment System. Finally, brittle deformation is related to normal faulting. Two normal faults are observed on Heraklia island. The Vourkaria fault, which trends NW-SE and dips towards to the northeast, and the Meriha fault, which trends NE-SW and dips towards to the northwest. Berhamnn and Seckel 2007, have characterized the Vourkaria fault as a reverse fault, however, structures related to reverse faulting have not been observed. Based on our observations, the Vourkaria fault is probably represent a normal fault and together with the Meriha normal fault form the graben of Heraklia island.

5.3. Metamorphic Events on Heraklia Island

Just like on most Cycladic islands, the CBU rocks of Heraklia island have experienced a greenschist retrogression, which has erased the previous HP metamorphic episode. However, relic of this HP event has been preserved in the southwestern part of the island. Glaucophane bearing rocks from the SW Heraklia have also been reported by Berhamann and Seckel 2007. Based on paleopiezometric analysis the same authors calculated the temperatures and differential stresses of the HP event at around 29-62 MPa and 400-450^{o} C, respectively. Similar observations have been described from the neighboring islands of Naxos and Ios. The rocks exposed on the SE Naxos have preserved the HP event, which was estimated at 350^{o} C at around 45$\pm$ 5 Ma (^{40}Ar/^{39}Ar, Wijbrans and McDougall 1988). On Ios island the P-T-t estimates place this event at 9-11 kbar, 350-400^{o} C between 40-50 Ma. Based on our new U-Pb detrital zircon dating the HP event on Heraklia island took place at around 50-55 Ma. These Eocene ages were obtained from the collected rocks from the SW part of the island. Therefore it is obvious that these islands share a quite common HP history. However, the retrogression differs, as on Naxos island the retrograde path reached the amphibolite facies conditions, while on Heraklia island the mineral composition has shown that it did not exceed the greenschist facies conditions. This second metamorphic event has affected the CBU rocks of Heraklia and as a result the structures related to the previous event have been overprinted.

5.4. U-Pb MDAs and Interpretation

The maximum depositional ages (MDAs) of detrital zircons from the metamorphic rocks from Herakla island point to a complicated tectonostratigraphy.

The analyzed zircons from the lowermost and uppermost lithological schist units have shown different zircon ages distributions and maximum depositional ages. We have found that the Paleozoic schists (~550 Ma) are dominated by Proterozoic zircon populations that range from 600 Ma to 2900 Ma. Interestingly, zircon ages younger than 550 Ma and metamorphic rims are not present on these schists. In addition, The

Paleozoic MDAs from the lowermost schists are similar to the U-Pb ages at about 500-560 Ma that have been reported from the basement rocks and its cover from the islands of Ios, Paros, Naxos and Sikinos (Keay and Lister 2002). Therefore, it could be assumed that the lowermost schists are related to the pre-Alpine basement and more specifically, they are part of the basement cover/carapace. On the contrary, the uppermost Late Cretaceous (~80 Ma) schists are mostly dominated by Paleozoic and little Pan- African zircon ages, and revealed a metamorphic rim at about 50 Ma, which is consistent with the ages of the high-pressure metamorphic event that took place between 55 and 34 Ma at a regional scale (Philippon et al., 2012).

Orthogneissic rocks

The orthogneissic rock samples have yielded Triassic MDAs at about 230 Ma. It is evident that Triassic ages approximately 220-245 Ma have also been determined for lenses of meta-acidic gneissic rocks within meta-sediments on Andros, Sifnos, Syros, Ios (Chatzaras et al., 2013, Liati et al., 2013, Brocker and Keasling 2006, Brocker and Pidgeon 2007), Naxos (Reischmann 1998), Evia (Chatzaras et al., 2013) and Attica (Lavrion) (Liati et al., 2009, Liati et al., 2013). Several authors have documented that the dominant scenario for this magmatic activity is related to a rifting setting, which took place during Late Permian to Early Triassic (Papanikolaou 1997, Stampfli 2000, Robertson 2011). Therefore, it could be assumed that the Triassic ages obtained from the orthogneissic rocks from Heraklia island are part of the magmatic activity that was widespread over large parts of the Attic-Cycladic zone throughout the Triassic.

5.4.1. PROVENANCE

Lowermost and uppermost lithological schist units

Seman et al., 2017 have distinguished two different zircon groups from the CBU rocks from the western Cycladic islands and Lavrion peninsula: i) the Proterozoic affinity with Triassic- Early Jurassic MDAs, and ii) the Paleozoic affinity with Late Jurassic-Cretaceous MDAs. Based on their study, the Proterozoic sediments have been derived from the northern Gondwanan margin, whereas, the Paleozoic sediments are sourced by the Internal Hellenides. The lithological schist units from Heraklia island share many similarities in terms of maximum depositional ages and zircon age distributions. Consequently, it could be assumed that the lowermost schists with Proterozoic affinity and with MDAs at about 550Ma from the central part of Heraklia island, have been sourced from the northern Gondwanan margin, whereas, the uppermost schists with Paleozoic affinity and Late Creataceous MDAs, are probably related to or sourced by the Internal Hellenides.

Finally, based on these zircon data and together with field observations and structural analysis, it is evident that the uppermost and lowermost schists correspond to two distinct lithological units, and they can not be part of the same unit as proposed by Berhmann and Seckel 2007.

5.5. SYNTHESIS

A correlation of U-Pb ages that obtained from the rock samples point to a complicated tectonostratigraphic evolution of Heraklia island. The different maximum depositional ages (MDAs) and zircon populations from the two lithological schist units provide evidence for a significant change in provenance. The Paleozoic lowermost quartz mica schists have derived from the eroded rocks of the Pan-African orogeny and they have been interpreted as part of the cover basement. The orthogneissic rocks, have intruded in the quartz mica schists during the Triassic, and together they represent the lowermost unit of Heraklia. The Late Cretaceous uppermost schists have shown that they are not related to the lowermost schists but instead, they are originated as sediments derived from the Internal Hellenides. The different MDAs indicate an age gap between the schist units, and therefore it demonstrates the presence of a detachment fault, which corresponds to the contact between the lowermost unit and the overlying marbles with uppermost schists. Just like on the central Cycladic islands of Naxos and Paros, this detachment fault displays an overall top to the north. Finally, the detachment fault from the northern Ios island shares common kinematics and separates the Cycladic Basement and the CBU rocks (Forster M. A. and Lister G.S., 1999). Therefore, assuming that part of the pre-alpine basement is exposed on the central part of Heraklia, the Heraklia Detachment is linked to the Naxos-Paros Detachment System, which separates the Cycladic Basement unit and the Cycladic Blueschist unit. The correlation between the detachment faults is schematically represented in figure 24.

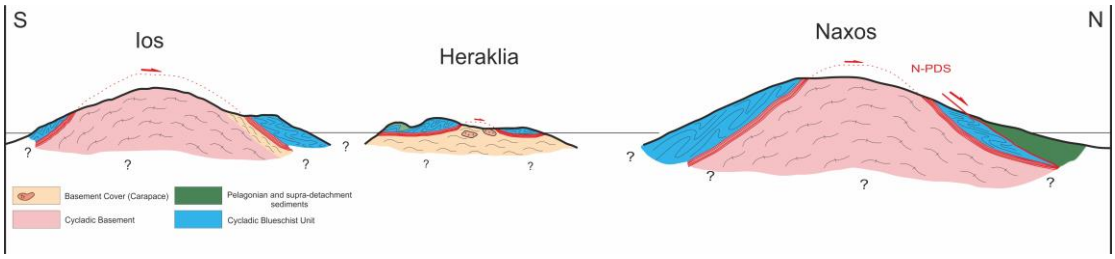

Figure 24: Schematic depiction of the detachment faults, separating the Cycladic Basement and the Cycladic Blueschist Units, and their probably connection on the islands of Ios, Heraklia and Naxos.

6. CONCLUSIONS

Based on these new U-Pb data we conclude that two distinct schist units are crop out on Heraklia island, which have shown evidence for different maximum depositional ages and provenance. The lowermost schists have been sourced from the northern Gondwana margin, in contrast with the uppermost schists that have been sourced from the units of the Internal Hellenides. Just like in the most parts of the Attic-Cycladic zone, the magmatic activity that took place during the Triassic has affected the CBU rocks of Heraklia island, and it is documented by the presence of orthogneissic rocks within the lowermost schists with maximum depositional ages at about 230 Ma.

Moreover, it is evident that the CBU rocks have experienced at least two metamorphic metamorphic events. The first one is related to the HP/LT facies conditions during the Eocene at about 50 Ma and it is evidenced by the presence of relic minerals, such as glaucophane, and the metamorphic rim that occurred in the uppermost schists from the U-Pb detrital zircon dating. The second one is related to the greenschists facies that resulted in the development of a penetrative foliation, isoclinal folding and a NW-SE to N-S stretching lineations. Finally, the stratigraphic age gap between the schists units have shown the existence of a detachment fault with top to the north kinematics, and it is related to the Paros-Naxos Detachment System.

REFERENCES

Altherr, R., Kreuzer, H., Wendt, I., Lenz, H., Wagner, G.A., Keller, J., Harre, W., Hohndorf, A., 1982. A Late Oligocene/Early Miocene high temperature belt in the anti-cycladic crystalline complex (SE Pelagonian, Greece). Geologisches Jahrbuch 23, 97–164.

Andriessen, P. A. M., G. Banga, and E. H. Hebeda (1987), Isotopic age study of pre-Alpine rocks in the basal units on Naxos, Sikinos and Ios, Greek Cyclades, Geol. Mijnbouw, 66, 3 – 14.

Angelier, J., 1977. Sur l' evolution tectonique depuis le Miocene superieur d' un arc insulaire mediterranee: l' arc Egeen. Rev. Geogr. Phys. Geol. Dyn. 19, 3, 271-294.

Angelier, J., Glaçon, G., Muller, C., 1978. Sur la présence et la position tectonique du Miocène inférieur marin dans l'archipel de Naxos (Cyclades, Grèce). Comptes Rendus. Académie des Sciences 286, 21–24.

Armijo, R., Meyer, B., Hubert, A., Barka, A., 1999. Westward propagation of the north Anatolian into the northern Aegean: timing and kinematics. Geology 27 (3), 267–270.

Augier, R., Jolivet, L., Gadenne, L., Lahfid, A., Driussi, O., 2014. Exhumation kinematics of the Cycladic Blueschists Unit and back-arc extension, insights from the Southern Cyclades (Sikinos and Folegandros Islands, Greece) Tectonics 34, 152–185.

Avigad, D., Garfunkel, Z., 1989. Low-angle faults above and below a blueschist belt: Tinos Island, Cyclades, Greece. Terra Nova 1, 182–187.

Avigad, D., Garfunkel, Z., 1991. Uplift and exhumation of high-pressure metamorphic terranes: The example of the Cycladic blueschists belt (Aegean Sea). Tectonophysics 188, 357–372.

Avigad, D., Ziv, A., Garfunkel, Z., 2001. Ductile and brittle shortening, extension-parallel folds and maintenance of crustal thickness in the Central Aegean. Tectonics 20 (2), 277–287.

Bargnesi, E. A., Stockli, D. F., Mancktelow, N., and Soukis, K., 2013, Miocene core complex development and coeval supradetachment basin evolution of Paros, Greece, insights from (U Th)/He thermochronometry: Tectonophysics, v.595-596, p. 165-182, dx. doi. org/110.1016/j. tecto.2012.1007.1015.

Barrell, J., (1917) Rhythms and the measurement of geologic time. Bulletin of the Geological Society of America 18: 745–904.

Bateman, H., (1910) Solution of a system of differential equations occurring in the theory of radioactive transformations. Proceedings of the Cambridge Philosophical Society 15: 423–427.

Bauer, C., Rubatto, D., Krenn, K., Proyer, A., Hoinkens, G., 2007. A zircon study from the Rhodope metamorphic complex, N-Greece: Time record of a multistage evolution. Lithos 99(2007) 207-228.

Beaudoin, A., Laurent, V., Augier, R., Jolivet, L., Lahfid, A., Arbaret, L., Rabillard, A., Menant, A., 2015. The Ikaria high-temperature metamorphic core complex (Cyclades, Greece): geometry, kinematics and thermal structure. J. Geodyn. 92, 18–41.

Behrmann, J.H., Seckel, C., 2007. Structures, flow stresses, and estimated strain rates in metamorphic rocks of the Small Cyclades Islands Iraklia and Schinoussa (Aegean Sea, Greece). Geotectonica Research 95, 1–11.

Boltwood BB (1907) On the ultimate disintegration products of the radioactive elements. Part II. The disintegration products of uranium. American Journal of Science 23: 77–88.

Bonev, N., Burg, J.P., Ivanov, Z., 2006. Mesozoic–Tertiary structural evolution of an extensional gneiss dome—the Kesebir–Kardamos dome, eastern Rhodope (Bulgaria–Greece). Int. J. Earth Sci. 95 (2), 318–340.

Böger H. Stratigraphische und tektonische Verknuepfungen kontinentaler Sedimente des Neogens im Aegais-Raum. Geologische Rundschau. 1983;72:771–813.

Bonneau, M., Kienast, J.R., 1982. Subduction, collision et schistes bleus: exemple de l'Egée, Grèce. Bull. Soc. géol. France 7, 785–791.

Bonneau, M., 1984. Correlation of the Hellenic nappes in the south-east Aegean and their tectonic reconstruction. In: Dixon, J.E., Robertson, A.H.F. (Eds.). The Geological Evolution of the Eastern Mediterranean. Special Publication of the Geological Society of London. Blackwell Scientific Publications, Oxford, pp. 517–527.

Brichau, S., Ring, U., Ketcham, R.A., Carter, A., Stockli, D., Brunel, M., 2006. Constraining the long-term evolution of the slip rate for a major extensional fault system in the central Aegean, Greece, using thermochronology. Earth and Planetary Science Letters 241, 293–306.

Brichau, S., Ring, U., Carter, A., Monie, P., Bolhar, R., Stockli, D., Brunel, M., 2007. Extensional faulting on Tinos Island, Aegean Sea, Greece: how many detachments? Tectonics 26, TC4009.

Brichau, S., Ring, U., Carter, A., Bolhar, R., Monié, P., Stockli, D., Brunel, M., 2008. Timing, slip rate, displacement and cooling history of the Mykonos detachment footwall, Cyclades, Greece, and implications for the opening of the Aegean Sea basin. J. Geol. Soc. London 165, 263–277.

Brichau, S., Thomson, S., Ring, U., 2010. Thermochronometric constraints on the tectonic evolution of the Serifos detachment, Aegean Sea, Greece. Int J Earth Sci (Geol Rundsch) 99, 379–393.

Bröcker, M., Keasling, A., 2006. Ion probe U–Pb zircon ages from the high pressure/low temperature mélange of Syros, Greece: age diversity and the importance of pre-Eocene subduction. Journal of Metamorphic Geology 24, 615–631.

Bröcker, M., Pidgeon, R.T., 2007. Protolith ages of meta-igneous and metatuffaceous rocks from the Cycladic Blueschist Unit, Greece: results of a reconnaissance U–Pb zircon study. Journal of Geology 115, 83–98.

Brodhag, S., Gracia-Calvo, M. & Schiwek, P., 2003: Geologie und Tektonik der Insel Iraklia/Kykladen (Griechenland). – Unpubl.nMapping Report, Univ. Freiburg, 76 pp.

Brun, J.P., Sokoutis, D., 2010. 45 m.y. of Aegean crust and mantle flow driven by trench retreat. Geology 38 (9), 815–818.

Buick, I. S. (1988), The metamorphic and structural evolution of the Barrovian overprint, Naxos, Cyclades, Greece, PhD thesis, 235 pp., Univ. of Cambridge, Cambridge, U. K.

Buick, I.S., Holland, T.J.B., 1989. The P–T–t path associated with crustal extension, Naxos, Cyclades, Greece. Geol. Soc. Lond. Spec. Publ. 43, 365–369.

Buick, I.S., 1991. Mylonite fabric development on Naxos, Greece. Journal of Structural Geology 13, 643–655.

Burg, J.P., Ricou, L.E., Ivano, Z., Godfriaux, I., Dimov, D., Klain, L., 1996. Syn-metamorphic nappe complex in the Rhodope Massif. Structure and kinematics. Terra Nova 8 (1), 6–15.

Chatzaras, V.,Dörr,W.,Finger, F.,Xypolias, P.,Zulauf, G., 2013. U–Pb single zircon ages and geochemistry of metagranitoid rocks in the Cycladic Blueschists (Evia Island): implications for the Triassic tectonic setting of Greece. Tectonophysics 595 (596), 125–139.

Denèle, Y., Lecomte, E., Jolivet, L., Lacombe, O., Labrousse, L., Huet, B., Le Pourhiet,L., 2011. Granite intrusion in a metamorphic core complex: the example of the Mykonos laccolith (Cyclades, Greece). Tectonophysics 501, 52–70.

Dewey, J. F., and Bird, J. M., 1970. Mountain belts and the new global tectonics. Journal of Geophysical Research, v.75, p. 2625-2647.

Dubois, R., Bignot, G., 1979. Présence d'un 'hardground' nummulitique au de la série Cretacée d'Almyropotamos (Eubée méridionale, Grèce). Comptes Rendus de l'Académie des Sciences, Série II 289, 993–995.

Duchene, S., Aissa, R., Vanderhaeghe, O., 2006. Pressure-temperature-time evolution of metamorphic rocks from Naxos (Cyclades, Greece): constraints from thermobarometry and Rb/Sr dating. Geodinamica Acta 19, 301–321.

Durr, S., E. Seidel, H. Kreuzer, and W. Harre (1978), Temoins d'un metamorphisme d'age cretace superieur dans l'Egeide: Datations radiometriques de mineraux provenant de l'ıle de Nikouria (Cyclades, Grece), Bull. Geol. Soc. Fr., 20, 209 – 213.

Engel, M., Reischmann, T., 1998. Single zircon geochronology of orthogneisses from Paros, Greece. Bulletin of the Geological Society of Greece 32/3, 91–99.

Faure, M., Bonneau, M., Pons, J., 1991. Ductile deformation and syntectonic granite emplacement during the late Miocene extension of the Aegean (Greece). Bull. Soc. géol. France 162, 3–12.

Ferrière, J., 1982. Paléogéographies et tectoniques superposées dans les Hellénides Internes: les massifs de l'Othrys et du Pélion (Grèce continentale). Société Géologique du Nord 7, 970.

Finetti, I., Papanikolaou, D., Del Ben, A., Karvelis, P., (1990). Preliminary geotectonic interpretation of the East Mediterranean chain and the Hellenic arc. Bulletin of the Geological Society of Greece vol. XXV/1, 509-526.1991.

Foster, M.A., Lister, G.S., 1999a. Detachment faults in the Aegean core complex of Ios, Cyclades, Greece. In: Ring, U., Brandon, M.T., Lister, G.S., Willett, S.D. (Eds.), Exhumation Processes: Normal Faulting, Ductile Flow and Erosion: Geological Society Special Publications. Geological Society, London, pp. 305–323.

Garfunkel, Z., C. A. Anderson, and G. Schubert, 1986: Mantle circulation and the lateral migration of subducted slabs, d. Geophys. Res., 91, 7205-7223.

Gautier, P., Brun, J.-P., Jolivet, L., 1993. Structure and kinematics of upper Cenozoic extensional detachment on Naxos and Paros (Cyclades Islands, Greece).Tectonics 12, 1180–1194.

Gautier, P., Brun, J.-P., 1994. Crustal-scale geometry and kinematics of late-orogenic extension in the central Aegean (Cyclades and Evia Island). Tectonophysics 238, 399–424.

Godfriaux, I., 1968. Etude geologique de la region de l'Olympe (Grece). Annales Geologiques des Pays Helleniques, v. 19 p. 1-280.

Godfriaux, I., Ricou, L.E., 1991. Direction et sens de transport associés au charriage synmétamorphe sur l'Olympe. Bulletin of the Geological Society of Greece 25, 207–229.

Grasemann, B., Petrakakis, K., 2007. Evolution of the Serifos Metamorphic Core Complex. In: Lister, G., Foster, M. (Eds.), Inside the Aegean Core Complexes. Journal of the Virtual Explorer, Electronic Edition.

Grasemann, B., Exner, U. & Tschegg, C. (2011): High-displacement gradients along ductily deforming brittle faults. Journal of Structural Geology, 33/11, 1650-1661. 10.1016/j.jsg. 2011.08.008.

Grasemann, B., Schneider, D.A., Stöckli, D.F., Iglseder, C., 2012. Miocene bivergent crustal extension in the Aegean: evidence from the western Cyclades (Greece).Lithosphere 4, 23–39.

Guernet, C., 1971. Etudes géologiques en Eubée et dans les régions voisines (Grèce). Thèse d'Etat Thesis, Université Paris VI, Paris.

Holmes A and Lawson RW (1927) Factors inolves in the calculation of the ages of radioactive minerals. American Journal of Science 13: 327–344.

Huet, B., Labrousse, L., Jolivet, L., 2009. Thrust or detachment? Exhumation processes in the Aegean: insight from a field study on Ios (Cyclades, Greece).Tectonics 28, TC3007.

Huet, B., 2010. Rhéologie de la lithosphère continentale: lexemple de la Mer Egée.Université Pierre et Marie Curie−Paris VI.

Iglseder, C., Grasemann, B., Schneider, D.A., Petrakakis, K., Miller, C., Klötzli, U.S., Thöni, M., Zámolyi, A., Rambousek, C., 2009. I and S-type plutonism on Serifos (W-Cyclades Greece). Tectonophysics 473, 69–83.

Iglseder, C., Grasemann, B., Rice, A.H.N., Petrakakis, K., Schneider, D.A., 2011. Miocene south directed low-angle normal fault evolution on Kea Island (West Cycladic detachment system, Greece). Tectonics 30, TC4013.

Jansen, J. B. H. (1977), Metamorphism on Naxos, Greece, thesis, Utrecht Univ., Utrecht, Netherlands.

Jansen, J.B.H., Schuiling, R.D., 1976. Metamorphism on Naxos: petrology and geothermal gradients. Am. J. Sci. 276 (10), 1225–1253.

Jolivet, L., Faccenna, C., 2000. Mediterranean extension and the Africa–Eurasia collision. Tectonics 19 (6), 1095–1106.

Jolivet, L., Augier, R., Faccenna, C., Negro, F., Rimmele, G., Agard, P., Robin, C., Rossetti, F., Crespo-Blanc, A., 2008. Subduction: convergence and the mode of backarc extension in the Mediterranean region. Bulletin de la Société Géologique de France 179, 525–550.

Jolivet, L., Brun, J.P., 2010. Cenozoic geodynamic evolution of the Aegean region. International journal of Earth Sciences 99, 109–138.

Jolivet, L., Lecomte, E., Huet, B., Denèle, Y., Lacombe, O., Labrousse, L., Le Pourhiet, L., Mehl, C., 2010. The North Cycladic detachment system. Earth Planet. Sci. Lett. 289, 87–104.

Jolivet, L., Faccenna, C., Huet, B., Labrousse, L., Le Pourhiet, L., Lacombe, O., Lecomte, E., Burov, E., Denèle, Y., Brun, J.-P., Philippon, M., Paul, A., Salaün, G., Karabulut, H., Piromallo, C., Monié, P., Gueydan, F., Okay, A.I., Oberhänsli, R., Pourteau, A., Augier, R., Gadenne, L., Driussi, O., 2012. Aegean tectonics: strain localisation, slab tearing and trench retreat. Tectonophysics 597-598, 1–33, http://dx.doi. org/10.1016/j.tecto.2012.06.011.

Jolivet, L., Menant, A., Sternai, P., Rabillard, A., Arbaret, L., Augier, R., Laurent, V., Beaudoin, A., Grasemann, B., Huet, B., Labrousse, L., Le Pourhiet, L., 2015. The geological signature of a slab tear below the Aegean. Tectonophysics 659, 166–182.

Kahle, H-G., Cocard, M., Peter, Y., Geiger, A., Reilinger, R., Barka, A., and Veis, G., 2000. GPS-derived strain rate field within the boundary zones of the Eurasian, African, and Arabian plates. Journal of Geophysical Reasearch vol. 105 NO. B10 pages 23,353-23,370.

Katsikatsos, G., De Bruijn, H., Van der Meulen, A.J., 1981. The Neogene of the island of Euboea (Evia), a review. Geologie en Mijnbouw 60, 509–516.

Katzir, Y., D. Avigad, A. Matthews, Z. Garfunkel, and B. W. Evans (1999), Origin and metamorphism of ultrabasic rocks associated with a subducted continental margin, Naxos (Cyclades, Greece), J. Metamorph. Geol., 17, 301–318.

Keay, S., 1998. The geological evolution of the Cyclades, Greece: constraints from SHRIMP U-Pb geochronology. PhD Thesis, Australian National University, Canberra, 341p.

Keay, S., Lister, G., Buick, I., 2001. The timing of partial melting, Barrovian metamorphism and granite intrusion in the Naxos metamorphic core complex Cyclades, Aegean Sea, Greece. Tectonophysics 342, 275–312.

Keay, S., Lister, G., 2002. African provenance for the metasediments and metaigneous rocks of the Cyclades, Aegean Sea, Greece. Geology 30 (3), 235–238.

Keiter, M., Piepjohn, K., Ballhaus, C., Lagos, M., Bode, M., 2004. Structural development of high-pressure metamorphic rocks on Syros island (Cyclades, Greece). J. Struct. Geol. 26 (8), 1433–1445.

Kuhlemann, J., Frisch, W., Dunkl, I., Kázmér, M., Schmiedl, G., 2004. Miocene siliciclastic deposits of Naxos Island: geodynamic and environmental implications for the evolution of the southern Aegean Sea (Greece). Geol. Soc. Am. Spec. Pap. 378, 51–65.

Kumerics, C., Ring, U., Brichau, S., Glodny, J., Monié, P., 2005. The extensional Messaria shear zone and associated brittle detachment faults, Aegean Sea, Greece. J. Geol. Soc. 162, 701–721.

Kydonakis, K., Gallagher, K., Brun, J.-P., Jolivet, M., Gueydan, F., Kostopoulos, D., 2014. Upper Cretaceous exhumation of the western Rhodope Metamorphic Province (Chalkidiki Peninsula, northern Greece). Tectonics 33 (6), 1113–1132. http://dx.doi.org/10.1002/2014TC003572 .

Laurent, V., Beaudoin, A., Jolivet, L., Arbaret, L., Augier, R., Rabillard, A., Menant, A., 2015. Interrelations between extensional shear zones and synkinematic intrusions: the example of Ikaria Island (NE Cyclades, Greece). Tectonophysics 651-652, 152–171.

Le Pichon, X., Angelier, J., 1981b. The Hellenic arc and trench system: a key to the neotectonic evolution of the eastern Mediterranean area. Philosophical Transactions of the Royal Society of London 300, 357–372.

Le Pichon, X., Lallemant, S.J., Chamot-Rooke, N., Lemeur, D., Pascal, G., 2002. The Mediterranean Ridge backstop and the Hellenic nappes. Mar. Geol. 186 (1–2), 111–125. http://dx.doi.org/10.1016/S0025-3227(02)00175-5.

Lecomte, E., Jolivet, L., Lacombe, O., Denèle, Y., Labrousse, L., Le Pourhiet, L., 2010. Geometry and kinematics of Mykonos detachment, Cyclades, Greece: evidence for slip at shallow dip. Tectonics 29.

Lee, J., Lister, G.S., 1992. Late Miocene ductile extension and detachment faulting, Mykonos, Greece. Geology 20, 121–124.

Lekkas, S., Skourtsos, Em., Soukis, K., Kranis, H., Lozios, S.G., Alexopoulos, A., Koutsovitis, P., 2011. Late Miocene detachment faulting and crustal extension in SE Attica (Greece). Geophysical Research Abstracts 13 (EGU-2011-13016).

Lenauer, I., Moertl, G., Iglseder, C., Grasemann, B. & Edwards, M. 2008. Field evidence for a major normal fault on Kythnos Island (Western Cyclades, Greece). Geophysical Research Abstracts, 10, EGU2008-A-03218.

Liati, A., Gebauer, D.,Wysoczanski, R., 2002. U–Pb SHRIMP-dating of zircon domains from UHP garnet-rich mafic rocks and late pegmatoids in the Rhodope zone (N Greece); evidence for Early Cretaceous crystallization and Late Cretaceous metamorphism. Chem. Geol. 184 (3–4), 281–299. http://dx.doi.org/10.1016/S0009-2541(01)00367-9.

Liati, A., Skarpelis, N., Pe-Piper, G., 2009. Late Miocene magmatic activity in the Attic–Cycladic Belt of the Aegean (Lavrion, SE Attica, Greece): implications for the geodynamic evolution and timing of ore deposition. Geol. Mag. 146 (5), 732–742.

Liati A., Skarpelis N., Mark Fanning C., (2013). Late Permian–Early Triassic igneous activity in the Attic Cycladic Belt (Attica): New geochronological data and geodynamic implications Tectonophysics 595–596, 140–147.

Lips, A. L. W., Wijbrans, J. R., and White S. H., 1999. New insights from 40Ar/39Ar laserprobe dating of white mica fabrics from the Pelion Massif, Pelagonian Zone, Internal Hellenides, Greece: implications for the timing of metamorphic episodes and tectonic events in the Aegean region. Geological Society, London, Special Publications, 156, 457-474, 1 January 1999, https://doi.org/10.1144/GSL.SP.1999.156.01.21.

Lister, G.S., Banga, G., Feenstra, A., 1984. Metamorphic core complexes of Cordilleran type in the Cyclades Aegean Sea, Greece. Geology 12, 221–225.

Lonergan L, White N. 1997. Origin of the Betic-Rif mountain belt. Tectonics 16:504–22.

Malinverno, A., Ryan, W.B.F., 1986. Extension in the Tyrrhenian Sea and shortening in the Apennines as result of arc migration driven by sinking of the lithosphere. Tectonics 5, 227–245.

McClusky, S., Balassanian, S., Barka, A., Demir, C., Ergintav, S., Georgiev, I., Gurkan, O., Hamburger, M., Hurst, K., Kahle, H., Kastens, K., Kekelidze, G., king, R., Kotzev, V., Lenk, O., Mahmoud, S., Mishin, A., Nadariya, M., Ouzonis, A., Paradissis, D., Peter, Y., Prilepin, M., Reilinger, R., Sanli, I., Seeger, H., Tealeb, A., Toksöz, M.N., Veis, G., 2000. Global Positioning System constraints on plate kinematics and dynamics in the eastern Mediterranean and Caucasus. Journal of Geophysical Research 105, 5695–5720.

McKenzie, D., 1978. Active tectonics of the Alpine–Himalayan belt: the Aegean Sea and surrounding regions. Geophysical Journal of the Royal Astronomical Society 55, 217–254.

Mehl, C., Jolivet, L., Lacombe, O., 2005. From ductile to brittle: evolution and localization of deformation below a crustal detachment (Tinos, Cyclades, Greece). Tectonics 24.

Melidonis, M.G., 1980. The geology of Greece: the geological structure and mineral deposits of Tinos Island (Cyclades, Greece). Institute of Geology and Mineral Exploration, Athens 13, 1–80.

Menant, A., Jolivet, L., Augier, R., Skarpelis, N., 2013. The North Cycladic Detachment System and associated mineralization, Mykonos, Greece: insights on the evolution of the Aegean domain. Tectonics 32, 433–452.

Menant, A., Jolivet, L., Vrielynck, B., 2016. Kinematic reconstructions and magmatic evolution illuminating crustal and mantle dynamics of the eastern Mediterranean region since the late Cretaceous. Tectonophysics.

Mercier, J.L., Carey, E., Philip, H., Sorel, D., 1976. La néotectonique plio-quaternaire de l'arc egéen externe et de la Mer égée et ses relations avec seismicité. Bulletin. Société Géologique de France 18, 159–176.

Morris A., and Anderson M., 1996. First paleomagnetic results from the Cycladic massif, Greece, and their implications for Miocene extension directions and tectonic models in the Aegean. Earth and Planetary Science Letters 142(1996) 397-408.

Nyst, M., and Thatcher, W., 2004. New constraints on the active tectonic deformation of the Aegean. JOURNAL OF GEOPHYSICAL RESEARCH, VOL. 109, B11406, doi: 10.1029 / 2003JB002830, 2004.

Papanikolaou, D.J., 1976. The age of the metamorphics in Andros island (Aegean Sea).

Papanikolaou, D.J., 1977. Contribution to the geology of the Aegean Sea: the island of Andros. Ann. Geol. Pays Hell. 29, 477–553.

Papanikolaou, D.J., 1978. Contribution to the geology of Aegean Sea. The Island of Andros. Annales Géologiques des Pays Hélléniques 29, 477–553.

Papanikolaou, D.J., 1979. Unités tectoniques et phases de déformations dans l'ile de Samos, Mer Egée, Grèce. Bulletin de la Société Géologique de France 21 (7), 745–762.

Papanikolaou, D.J., 1980. Contribution to the geology of the Aegean Sea. The island of Paros. Annales Géologiques des Pays Helléniques 30/1, 65–96.

Papanicolaou, D.J., (1986). Geology of Greece. Eptalofos Ltd, Athens (in Greek).

Papanikolaou, D.J., 1989. Are the medial crystalline massifs of the eastern Mediterranean drifted Gondwanan fragments? Geological Society of Greece Special Publication 1, 63–90.

Papanikolaou, D.J., E. Logos, S. Lozios, and C. Sideris (1997), Korinthos, in Neotectonic Map of Greece, scale 1:100,000, Earthquake Plann. And Prot. Organ., Athens.

Papanikolaou, D.J., and Royden, L., 2007. Disruption of the Hellenic arc: Late Miocene extensional detachment faults and steep Pliocene- Quaternary normal faults- Or what happened at Corinth? Tectonics VOL. 26, TC5003, doi:10.1029/2006TC002007, 2007.

Papanikolaou, D.J., 2009. Timing of tectonic emplacement of the ophiolites and terrane paleogeography in the Hellenides. Lithos, 108, 262-280.

Petrus,J. A., and Kamber, B. S., 2012. Vizual age: A novel approach to laser ablation ICP-MS U-Pb geochronology data reduction, Geostand. Geoanal. Res., 36, 247-270.

Philippon, M., Brun, J.-P., Gueydan, F., 2011. Tectonics of the Syros blueschists (Cyclades Greece): from subduction to Aegean extension. Tectonics 30 (4).

Philippon, M., Brun, J.P., Gueydan, F., 2012. Deciphering subduction from exhumation in the segmented Cycladic Blueschist Unit (Central Aegean, Greece). Tectonophysics 524–525, 116–134.

Philippon, M., Brun, J.P., Gueydan, F., Sokoutis, D., 2014. The interaction between Aegean back-arc extension and Anatolia escape since Middle Miocene. Tectonophysics 631, 176–188.

Reinecke, T., Altherr, R., Hartung, B., Hatzipanagiotou, K., Kreuzer, H., Harre, W., Klein, H., Keller, J., Geenen, E., Böger, H., 1982. Remnants of a late Cretaceous high temperature belt on the island of Anafi (Cyclades, Greece). Neus Jahrbuch fur Mineralogie Abhandlungen 145, 157–182.

Reischmann, T., 1998. Pre-Alpine origin of tectonic units from the metamorphic complex of Naxos, Greece, identified by single zircon Pb/Pb dating, Bull. Geol. Soc. Gr., 32, 101–111.

Ring, U., Gessner, K., Güngör, T., Passchier, C.W., 1999a. The Menderes massif of western Turkey and the Cycladic massif in the Aegean: do they really correlate? Journal of the Geological Society of London 156, 3–6.

Ring, U., Laws, S., Bernet, M., 1999b. Structural analysis of a complex nappe sequence and late-orogenic basins from the Aegean Island of Samos, Greece. Journal of Structural Geology 21, 1575–1601.

Ring, U., Layer, P.W., Reischmann, T., 2001. Miocene high-pressure metamorphism in the Cyclades and Crete, Aegean Sea, Greece: evidence for large-magnitude displacement on the Cretan detachment. Geology 29 (5), 395.

Ring, U., Layer, P.W., 2003. High-pressure metamorphism in the Aegean, eastern Mediterranean: underplating and exhumation from the Late Cretaceous until the Miocene to Recent above the retreating Hellenic subduction zone. Tectonics 22 (3).

Ring, U., Glodny, J., Will, T., Thomson, S., 2007a. An Oligocene extrusion wedge of blueschists-facies nappes on Evia, Aegean Sea, Greece: implications for the early exhumation of high-pressure rocks. Journal of the Geological Society of London 164, 637–652.

Ring, U., Will, T., Glodny, J., Kumerics, C., Gessner, K., Thomson, S., Güngör, T., Monie, P., Okrusch, M., Drüppel, K., 2007b. Early exhumation of high-pressure rocks in extrusion wedges: Cycladic blueschist unit in the eastern Aegean, Greece, and Turkey. Tectonics 26, TC2001.

Ring, U., Glodny, J., Will, T., Thomson, S., 2010. The Hellenic subduction system: high-pressure metamorphism, exhumation, normal faulting, and large-scale extension. Annu. Rev. Earth Planet. Sci. 38, 45–76.

Ring, U., Glodny, J., Will, T.M., Thomson, S., 2011. Normal faulting on Sifnos and the south Cycladic detachment system, Aegean Sea, Greece. J. Geol. Soc. 168,751–768

Robertson, A.H.F., 2011. Late Palaeozoic–Cenozoic tectonic development of Greece and Albania in the context of alternative reconstructions of Tethys in the Eastern Mediterranean region. International Geology Review 1–8.

Roche, V., Laurent, V., Cardello, G.L., Jolivet, L., Scaillet, S., 2016. Anatomy of the Cycladic Blueschist Unit on Sifnos Island (Cyclades, Greece). J. Geodyn.

Royden, L. H. (1993), Evolution of retreating subduction boundaries formed during continental collision, Tectonics, 12(3), 629–638, doi: 10.1029/92TC02641.

Royden, L.H., Papanikolaou, D.J., 2011. Slab segmentation and late Cenozoic disruption of the Hellenic arc. Geochemistry, Geophysics, Geosystems 12 (3), Q03010.

Sanchez-Gomez, M., Avigad, D., Heimann, A., 2002. Geochronology of clasts in allochthonous Miocene sedimentary sequences on Mykonos and Paros Islands: implications for back-arc extension in the Aegean Sea. J. Geol. Soc. 159, 45–60.

Schoene, B., 2014. 4.10-U-Th-Pb Geochronology. Treatise on Geochemistry 2nd edition, vol. 4 pages 341-378.

Seckel, C., 2004: Strukturgeologische Untersuchungen auf den Kykladeninseln Iraklia und Schinoussa, Griechenland. – DiplomanThesis, Univ. Freiburg, 131 pp.

Seman, S., Stockli, F. D., and Soukis, K., 2017. The provenance and internal structure of the Cycladic Blueschist Unit revealed by detrital zircon geochronology, Western Cyclades, Greece. Tectonics, 36, doi:10.1002/2016TC004378.

Seward, D., Vanderhaeghe, O., Siebenaller, L., Thomson, S., Hibsch, C., Zingg, A., Holzner, P., Ring, U., Duchêne, S., 2009. Cenozoic tectonic evolution of Naxos Island through a multi-faceted approach of fission-track analysis. In: Ring, U., Wernicke, B. (Eds.), Extending a Continent: Architecture, Rheology and Heat Budget vol. 321. Geological Society, London, pp. 179–196.

Shaked, Y., Avigad, D., Garfunkel, Z., 2000. Alpine high-pressure metamorphism of the Almyropotamos window (southern Evia, Greece). Geological Magazine 137 (4), 367–380.

Sokoutis, D., Brun, J.P., Driessche, J.V.D., Pavlides, S., 1993. A major Oligo-Miocene detachment in southern Rhodope controlling north Aegean extension. Journal of Geological Society of London 150, 243–246.

Sotiropoulos, S., Kamberis, E., Triantaphyllou,M.V., Doutsos, T., 2003. Thrust sequences in the central part of the External Hellenides. Geological Magazine 140, 661–668.

Soukis, K., Papanikolaou, J.D., 2004. Contrasting geometry between Alpine and late- to post-Alpine tectonic structures in Anafi Island (Cyclades). Bulletin of the Geological Society Greece XXXVI, 1688–1696.

Soukis K., and Stockli F. D., 2013. Structural and thermochronometric evidence for multi-stage exhumation of southern Syros, Cycladic islands, Greece. Tectonophysics 595-596 (2013) 148-164.

Stampfli, G. M., 2000. Tethyan oceans. In: Bozkurt, E., Winchester, J.A., Piper, J.D.A. (Eds.), Tectonics and Magmatism in Turkey and Surrounding Region: Geol. Soc. London Spec. Publ., 173, pp. 1–23.

Theodoropoulos, D., 1979. Samos island. Geological map of Greece, scale 1/50000 I.G.M.E. Athens.

Thomson, S.N. Stöckhert, B. Rauche, H. Brix, M.R., 1998a. Apatite fission-track thermochronology of the uppermost tectonic unit of Crete, Greece: implications for the post-Eocene tectonic evolution of the Hellenic subduction system. In: van den Haute, P., de Corte F. (Eds.). Advances in Fission-track Geochronology, Kluwer Academic Publishers, Dortrecht, pp. 187-205.

Thomson, S.N., Ring, U., Brichau, S., Glodny, J., Will, T.M., 2009. Timing and nature of formation of the Ios metamorphic core complex, southern Cyclades, Greece. In: Ring, U., Wernicke, B. (Eds.), Extending a Continent: Architecture, Rheology and Heat Budget: Geological Society, Special Publications, London, pp. 139–167.

Tremblay, A., Meshi, A., Deschamps, T., Goulet, F., Goulet, N., 2015. The Vardar zone as a suture for the Mirdita ophiolites, Albania: Constraints from the structural analysis of the Korabi-Pelagonian zone. Tectonics, 34, 352-375, doi:10.1002/2014TC003807.

Tschegg, C., Grasemann, B., 2009. Deformation and alteration of a granodiorite during low-angle normal faulting (Serifos, Greece). Lithosphere 1 (3), 139–154.

Underhill, J.R., 1989: Late Cenozoic deformation of the Hellenide foreland, western Greece. Geol. Soc. Am. Bull., 101, 613–634.

Urai, J.L., Schuiling, R.D., Jansen, J.B.H., 1990. Alpine deformation on Naxos (Greece). Geol. Soc. London Spec. Publ. 54 (1), 509–522.

Van Hinsbergen, D., Hafkenscheid, E., Spakman, W., Meulenkamp, J.E., Wortel, R., 2005a. Nappe stacking resulting from subduction of oceanic and continental lithosphere below Greece. Geology 33, 325–328.

Van Hinsbergen, D.J.J., Langereis, C.G., Meulenkamp, J.E., 2005b. Revision of the timing, magnitude and distribution of Neogene rotations in the western Aegean region. Tectonophysics 396 (1–2), 1–34.

Van Hinsbergen, D.J.J., and Schmid, S., 2012. Map view restoration of Aeagean- West Anatolian accretion and extension since the Eocene. Tectonics, vol. 31, TC5005, doi: 10.1029/2012TC003132.

Vermeesch, P., 2004. How many grains are needed for a provenance study? Earth and Planetary Science Letters, vol. 224, pages 441-451.

Von Quadt, A., Moritz, R., Peytcheva, I., Heinrich, C.A., 2005. 3: Geochronology and geodynamics of Late Cretaceous magmatism and Cu–Au mineralization in the Panagyurishte region of the Apuseni–Banat–Timok–Srednogorie belt, Bulgaria. Ore Geol. Rev. 27 (1–4), 95–126.

Walcott, C.R., White, S.H., 1998. Constraints on the kinematics of post-orogenic extension imposed by stretching lineations in the Aegean region. Tectonophysics 298, 155–175.

Wetherill GW (1956) Discordant uranium–lead ages. Transactions of the American Geophysical Union 37: 320–326.

Wijbrans, J.R., and McDougall, I., 1988. Metamorphic evolution of the Attic Cycladic Metamorphic belt on Naxos (Cyclades, Greece) utilizing J"Ar/.79Ar age spectrum measurements. Metamorph. Geol. 6 (1988) 57 I-594.

Wüthrich, E.D., 2009. Low temperature thermochronology of the northern Aegean Rhodope Massif. A dissertation submitted to the, Swiss Federal Institute of Technology Zürich.

Ziv, A., Katzir, Y., Avigad, D., Garfunkel, Z., 2010. Strain development and kinematic significance of the Alpine folding on Andros (western Cyclades, Greece). Tectonophysics 488 (1–4), 248–255.

Zulauf G., W. Dörr W., Fisher-Spurlock S.C., Gerdes A., Chatzaras V., Xypolias P., (2015). Closure of the Paleotethys in the External Hellenides: Constraints from U–Pb ages of magmatic and detrital zircons (Crete). Gondwana Research 28 (2015) 642–667.

APPENDIX

Table 2: U-Pb analytical data from zircons, Heraklia Island, Cyclades.

Sample Name:					**Best age**
Grain	**[U] ppm**	**U/Th**	**207/235**	**206/238**	**(Ma)**
IRA1503_1.FIN2	71.4	0.84	1.78600	0.17340	1069.0
IRA1503_3.FIN2	158	2.35	1.43100	0.15240	867.0
IRA1503_4.FIN2	346	3.11	5.00800	0.31880	1874.0
IRA1503_4.FIN2	596	11.60	6.98800	0.36740	2200.0
IRA1503_5.FIN2	89.5	0.79	10.36000	0.46750	2469.0
IRA1503_6.FIN2	41.84	1.22	10.13000	0.46660	2420.0
IRA1503_7.FIN2	100.8	0.74	11.43000	0.49700	2523.0
IRA1503_8.FIN2	67.6	1.31	1.14700	0.12180	741.0
IRA1503_10.FIN2	193	1.32	1.22600	0.13290	804.3
IRA1503_11.FIN2	164	1.46	10.94000	0.46930	2544.0
IRA1503_12.FIN2	405	1.63	1.22600	0.13302	805.0
IRA1503_13.FIN2	226	1.87	9.15700	0.40870	2479.0
IRA1503_14.FIN2	1229	5.33	12.82400	0.51550	2652.0
IRA1503_15.FIN2	529	1.15	11.70300	0.50690	2538.5
IRA1503_16.FIN2	564	2.13	1.13800	0.12660	768.6
IRA1503_17.FIN2	173.3	1.17	0.84300	0.10137	623.5
IRA1503_19.FIN2	235	5.79	5.37100	0.34600	1837.0

IRA1503_20.FIN2	88.4	0.70	0.87300	0.10420	638.8
IRA1503_21.FIN2	77.6	0.54	1.38100	0.14580	902.0
IRA1503_22.FIN2	245.3	5.82	5.73400	0.35880	1881.0
IRA1503_23.FIN2	152.5	1.38	11.78000	0.50750	2540.0
IRA1503_24.FIN2	418	1.18	0.87000	0.10420	639.7
IRA1503_25.FIN2	50.6	1.21	1.13100	0.12210	742.0
IRA1503_26.FIN2	176	1.17	1.46600	0.15190	916.0
IRA1503_27.FIN2	285	4.25	10.86000	0.47290	2515.0
IRA1503_28.FIN2	281.1	3.86	8.34000	0.37600	2457.0
IRA1503_29.FIN2	858	16.99	11.20400	0.48530	2533.7
IRA1503_30.FIN2	387	1.03	1.76000	0.17420	1019.0
IRA1503_31.FIN2	287.1	1.84	1.68500	0.16880	983.0
IRA1503_32.FIN2	793	10.15	13.86100	0.52430	2752.0
IRA1503_33.FIN2	163	0.75	1.23000	0.13530	817.8
IRA1503_34.FIN2	339	0.97	1.59600	0.16220	970.0
IRA1503_36.FIN2	430	6.23	8.31900	0.37400	2469.0
IRA1503_37.FIN2	493	3.80	5.56900	0.35160	1886.0
IRA1503_38.FIN2	196.8	0.77	1.16700	0.12830	778.1
IRA1503_39.FIN2	627.5	1.30	9.94000	0.44530	2481.0
IRA1503_40.FIN2	453	5.90	1.71000	0.17350	968.0
IRA1503_41.FIN2	159.1	0.71	9.70000	0.43310	2484.0
IRA1503_42.FIN2	35.6	0.66	13.39000	0.52140	2700.0
IRA1503_43.FIN2	656	1.18	1.22500	0.13480	815.2
IRA1503_44.FIN2	345	1.10	1.22000	0.13350	808.4
IRA1503_45.FIN2	494	0.77	1.21700	0.13415	812.1
IRA1503_46.FIN2	88.9	0.60	1.00000	0.11570	706.0
IRA1503_47.FIN2	311	1.02	1.19800	0.13060	791.2
IRA1503_48.FIN2	684	7.21	10.15000	0.44420	2498.0
IRA1503_49.FIN2	110.9	0.91	1.15800	0.12890	783.0
IRA1503_50.FIN2	221.5	0.96	1.21600	0.13330	808.0
IRA1503_51.FIN2	135.7	0.61	10.88100	0.48150	2480.0

IRA1503_53.FIN2	174.6	0.47	1.24900	0.13270	804.1
IRA1503_54.FIN2	276	0.97	1.30400	0.14000	844.4
IRA1503_55.FIN2	541	1.12	10.77600	0.46410	2531.0
IRA1503_56.FIN2	168	0.92	1.18200	0.12950	785.1
IRA1503_57.FIN2	332.2	3.56	1.64700	0.16450	976.0
IRA1503_58.FIN2	1590	1.03	0.85200	0.10170	624.3
IRA1503_59.FIN2	280	0.88	0.79600	0.09640	593.2
IRA1503_60.FIN2	586	2.65	9.68600	0.44110	2434.0
IRA1503_61.FIN2	104.3	0.62	1.22700	0.13180	797.7
IRA1503_62.FIN2	42.41	1.33	2.69100	0.21130	1510.0
IRA1503_63.FIN2	130.4	1.16	8.33000	0.37680	2445.0
IRA1503_64.FIN2	198	9.60	13.52000	0.52510	2709.0
IRA1503_65.FIN2	251	0.94	2.68200	0.21190	1466.0
IRA1503_66.FIN2	280.6	2.55	11.34900	0.48870	2535.0
IRA1503_67.FIN2	241.6	1.58	1.20600	0.13410	811.0
IRA1503_68.FIN2	238	1.46	0.76200	0.09210	567.7
IRA1503_69.FIN2	141.3	1.26	0.87600	0.10510	644.0
IRA1503_70.FIN2	311.4	0.99	10.37200	0.45700	2511.0
IRA1503_71.FIN2	85.5	1.16	1.22400	0.13120	794.6
IRA1503_73.FIN2	204	1.58	1.01300	0.11330	692.0
IRA1503_75.FIN2	119.9	1.86	9.41100	0.42470	2472.0
IRA1503_76.FIN2	364	1.86	0.43500	0.05300	333.0
IRA1503_77.FIN2	1262	9.20	9.84000	0.42920	2520.0
IRA1503_78.FIN2	102.2	2.30	0.89700	0.10270	630.0
IRA1503_79.FIN2	552	6.03	5.25000	0.33560	1858.0
IRA1503_80.FIN2	220	1.98	11.15000	0.48190	2534.0
IRA1503_81.FIN2	86.3	0.67	0.79100	0.09820	603.8
IRA1503_82.FIN2	108.9	1.11	1.03900	0.11280	689.0
IRA1503_83.FIN2	278	3.64	9.29000	0.41060	2496.0
IRA1503_84.FIN2	271	4.82	1.55400	0.16100	926.0
IRA1503_85.FIN2	64.3	0.52	11.15000	0.47980	2530.0

IRA1503_86.FIN2	128.3	1.50	4.61300	0.27060	1986.0
IRA1503_87.FIN2	120.8	0.68	1.23700	0.13710	828.1
IRA1503_88.FIN2	430	3.43	6.39500	0.36830	2038.0
IRA1503_89.FIN2	336	0.64	0.79800	0.09550	587.7
IRA1503_90.FIN2	129.4	1.22	1.21900	0.13310	805.5
IRA1503_91.FIN2	905	1.56	1.26300	0.13640	824.2
IRA1503_92.FIN2	271	0.90	1.19100	0.12970	786.2
IRA1503_93.FIN2	301	3.35	12.16000	0.50000	2618.0
IRA1503_94.FIN2	148	1.34	0.86400	0.10170	625.4
IRA1503_96.FIN2	23.03	8.40	10.47000	0.46600	2483.0
IRA1503_98.FIN2	74.6	0.50	6.30000	0.36220	2048.0
IRA1503_99.FIN2	140	1.30	1.30500	0.14000	844.7
IRA1503_100.FIN2	72.8	0.77	11.06000	0.47980	2539.0
IRA1503_101.FIN2	76	0.52	1.18500	0.12810	777.0
IRA1503_102.FIN2	30	2.13	9.46000	0.43500	2434.0
IRA1503_104.FIN2	143.9	0.72	1.36700	0.14350	897.0
IRA1503_105.FIN2	335	1.07	1.34300	0.13870	838.0
IRA1503_106.FIN2	490	0.62	0.73780	0.08997	555.3
IRA1503_107.FIN2	141.6	0.79	10.98000	0.47330	2540.0
IRA1503_109.FIN2	877	4.07	13.09000	0.49340	2760.0
IRA1503_110.FIN2	227	1.25	0.99700	0.11520	702.9
IRA1503_111.FIN2	143.2	4.15	6.16600	0.37110	1972.0
IRA1503_112.FIN2	296	5.47	5.46300	0.34650	1882.0
IRA1503_113.FIN2	466	0.50	1.00200	0.11150	682.0
IRA1503_114.FIN2	195	0.29	0.78200	0.09550	587.8
IRA1503_116.FIN2	275.7	0.91	15.76000	0.56610	2846.0
IRA1503_117.FIN2	540.7	0.34	0.92400	0.09663	DISC
IRA1503_118.FIN2	244.1	2.15	6.23000	0.36660	1999.0
IRA1503_119.FIN2	295.4	0.51	0.75900	0.09130	563.2
IRA1503_120.FIN2	98.8	0.71	1.04000	0.11900	724.4
IRA1512_1.FIN2	427	0.82	0.90500	0.10700	655.3

IRA1512_2.FIN2	296	1.75	0.85700	0.10130	622.1
IRA1512_3.FIN2	105.5	1.14	1.73900	0.16610	1087.0
IRA1512_4.FIN2	231.7	2.05	0.85900	0.10279	631.1
IRA1512_5.FIN2	41.2	0.77	0.85000	0.10240	628.0
IRA1512_6.FIN2	530	1.20	0.37450	0.04983	313.4
IRA1512_7.FIN2	127	2.91	0.86400	0.10390	637.0
IRA1512_9.FIN2	614	0.64	0.26540	0.03797	240.2
IRA1512_10.FIN2	76.2	0.91	5.42800	0.34590	1856.0
IRA1512_11.FIN2	732	3.15	1.86000	0.17390	1112.0
IRA1512_13.FIN2	107.1	3.93	9.48000	0.41460	2512.0
IRA1512_14.FIN2	80.5	0.89	1.09000	0.12240	744.4
IRA1512_15.FIN2	69.4	0.95	0.85900	0.10330	633.4
IRA1512_16.FIN2	569	0.88	0.26860	0.03659	231.6
IRA1512_17.FIN2	315	0.42	0.83900	0.10010	614.8
IRA1512_18.FIN2	88.2	2.67	1.10100	0.12640	767.0
IRA1512_19.FIN2	1269	40.30	1.46700	0.15010	958.0
IRA1512_20.FIN2	646	0.67	0.27340	0.03755	237.6
IRA1512_21.FIN2	805	0.78	0.24670	0.03579	226.7
IRA1512_22.FIN2	232.5	0.91	1.46900	0.15130	953.0
IRA1512_23.FIN2	194.6	0.68	1.09600	0.12080	734.9
IRA1512_24.FIN2	68.8	2.07	1.60400	0.16470	949.0
IRA1512_25.FIN2	179.1	2.07	1.54000	0.15870	920.0
IRA1512_26.FIN2	120.5	1.04	11.19700	0.49320	2510.0
IRA1512_27.FIN2	583	2.37	11.01900	0.48630	2511.0
IRA1512_28.FIN2	875	0.60	0.25730	0.03658	231.6
IRA1512_29.FIN2	481	0.61	0.26580	0.03770	238.5
IRA1512_30.FIN2	493.4	1.92	1.79300	0.17760	1042.0
IRA1512_31.FIN2	108.3	0.63	1.33300	0.14350	874.0
IRA1512_32.FIN2	327	1.13	6.26800	0.37360	1991.0
IRA1512_33.FIN2	740	0.80	0.25190	0.03610	228.6
IRA1512_34.FIN2	74.7	1.93	2.07800	0.19880	1089.0

IRA1512_35.FIN2	561	1.92	1.56900	0.15240	1060.0
IRA1512_36.FIN2	1066	1.65	0.27410	0.03892	246.1
IRA1512_37.FIN2	48.2	0.28	5.97000	0.35630	2009.0
IRA1512_37.FIN2	47.2	0.64	10.37000	0.44700	2555.0
IRA1512_38.FIN2	270	1.16	1.23200	0.13490	816.0
IRA1512_39.FIN2	184.6	4.66	12.61000	0.49420	2699.0
IRA1512_40.FIN2	232	1.19	0.94500	0.11178	683.0
IRA1512_41.FIN2	31.8	1.26	1.16900	0.12650	767.0
IRA1512_42.FIN2	174	1.09	11.76000	0.49080	2590.0
IRA1512_43.FIN2	373	22.50	1.40300	0.14850	861.0
IRA1512_44.FIN2	421	1.79	1.20700	0.13420	811.5
IRA1512_45.FIN2	223	1.12	1.12800	0.12600	765.0
IRA1512_46.FIN2	212	1.55	11.55000	0.48430	2576.0
IRA1512_47.FIN2	1035	1.41	0.27340	0.03858	244.0
IRA1512_48.FIN2	871	3.99	0.81300	0.09990	614.0
IRA1512_49.FIN2	650	21.00	0.65600	0.08240	510.0
IRA1512_50.FIN2	86.1	1.09	1.63100	0.16420	979.0
IRA1512_51.FIN2	404.8	2.60	0.64000	0.07976	494.7
IRA1512_52.FIN2	134.2	0.58	5.46300	0.34370	1881.0
IRA1512_53.FIN2	158.6	4.28	1.31000	0.14010	845.0
IRA1512_54.FIN2	97.2	1.39	10.96000	0.47940	2517.0
IRA1512_55.FIN2	168	0.60	1.82100	0.17670	1068.0
IRA1512_56.FIN2	154.1	3.54	0.94900	0.11230	686.1
IRA1512_58.FIN2	225.8	1.53	1.56600	0.15870	984.0
IRA1512_59.FIN2	134.7	2.81	5.89000	0.33670	2068.0
IRA1512_60.FIN2	83	0.46	0.70100	0.08780	543.6
IRA1512_61.FIN2	659	12.26	0.73600	0.08840	545.8
IRA1512_62.FIN2	232	1.41	1.85300	0.18240	1043.0
IRA1512_63.FIN2	104	0.81	1.52800	0.15900	938.0
IRA1512_64.FIN2	269.1	1.34	1.82500	0.17610	1074.0
IRA1512_65.FIN2	165.3	1.87	0.41120	0.05420	340.2

IRA1512_66.FIN2	75	1.18	1.56100	0.15640	978.0
IRA1512_67.FIN2	536	2.08	0.86380	0.10384	636.8
IRA1512_68.FIN2	121.6	2.09	0.86400	0.10190	626.6
IRA1512_69.FIN2	152.9	1.42	5.37700	0.32970	1949.0
IRA1512_70.FIN2	306	1.79	1.11200	0.12330	749.4
IRA1512_71.FIN2	768	1.71	0.26600	0.03765	238.2
IRA1512_72.FIN2	964	10.80	0.39100	0.05010	315.0
IRA1512_72.FIN2	50.3	0.54	4.18800	0.29030	1727.0
IRA1512_73.FIN2	114.2	1.54	1.28300	0.13960	843.1
IRA1512_74.FIN2	375	1.52	0.26300	0.03847	243.3
IRA1512_74.FIN2	522	1.77	0.99500	0.11310	690.9
IRA1512_75.FIN2	55.4	2.01	1.45900	0.14850	962.0
IRA1512_76.FIN2	333	1.76	0.86300	0.10290	631.5
IRA1512_77.FIN2	186.9	1.65	1.31300	0.14140	844.0
IRA1512_78.FIN2	262	1.38	0.70900	0.08810	544.0
IRA1512_78.FIN2	444	2.02	2.33200	0.19780	1338.0
IRA1512_79.FIN2	478	2.97	0.96700	0.10920	668.0
IRA1512_79.FIN2	809	1.37	2.53500	0.18530	DISC
IRA1512_80.FIN2	251.6	1.46	1.31400	0.13960	842.0
IRA1512_81.FIN2	16.8	1.71	5.75000	0.34700	1911.0
IRA1512_81.FIN2	59.5	2.91	11.36000	0.51100	2452.0
IRA1512_82.FIN2	332	3.99	0.86300	0.10240	628.6
IRA1512_83.FIN2	155	1.32	0.85900	0.10270	629.9
IRA1512_84.FIN2	521	0.84	0.25970	0.03685	233.3
IRA1512_85.FIN2	185.6	1.86	8.53700	0.38460	2439.0
IRA1512_86.FIN2	35.8	0.84	0.77900	0.09540	589.0
IRA1512_87.FIN2	611	1.31	0.69000	0.08320	514.9
IRA1512_88.FIN2	234	0.85	0.87800	0.10398	637.6
IRA1512_89.FIN2	59.2	1.88	0.26800	0.04000	252.8
IRA1512_90.FIN2	176	1.65	0.89300	0.10480	642.6
IRA1512_91.FIN2	335.6	0.80	0.28770	0.03609	DISC

IRA1512_92.FIN2	341	1.39	0.76300	0.09060	558.7
IRA1512_93.FIN2	58.9	1.61	1.55800	0.16040	935.0
IRA1512_94.FIN2	1284	1.97	0.69590	0.08580	530.7
IRA1512_95.FIN2	540	6.22	1.49700	0.15470	936.0
IRA1512_96.FIN2	89.5	0.93	1.12100	0.12630	766.7
IRA1512_97.FIN2	265.3	0.74	1.10600	0.12350	750.4
IRA1512_98.FIN2	32.27	11.20	0.28300	0.03910	247.2
IRA1512_99.FIN2	302	0.58	0.25950	0.03663	231.9
IRA1512_100.FIN2	209.4	1.32	26.86000	0.67970	3401.0
IRA1512_101.FIN2	340	0.36	1.09800	0.12270	745.8
IRA1512_102.FIN2	203	1.77	1.61200	0.16550	974.0
IRA1512_103.FIN2	314	1.14	1.15000	0.12880	781.0
IRA1512_105.FIN2	357.3	2.01	0.80000	0.09791	602.1
IRA1512_106.FIN2	419.6	0.84	0.25570	0.03705	234.5
IRA1512_107.FIN2	426	0.81	0.26700	0.03819	241.6
IRA1512_108.FIN2	685	0.78	0.25130	0.03625	229.5
IRA1512_109.FIN2	705	1.09	0.26540	0.03812	241.2
IRA1512_110.FIN2	416	2.91	1.55100	0.15710	965.0
IRA1512_111.FIN2	334	1.60	0.89700	0.10670	653.2
IRA1512_112.FIN2	114.9	1.45	1.74600	0.17470	999.0
IRA1512_113.FIN2	343	3.31	1.14400	0.12690	770.1
IRA1512_114.FIN2	88.6	0.95	0.79400	0.09690	595.9
IRA1512_115.FIN2	754	3.85	0.78490	0.09603	591.0
IRA1512_116.FIN2	150.6	1.97	0.95500	0.11072	676.9
IRA1512_117.FIN2	149	1.75	12.99000	0.52160	2655.0
IRA1512_118.FIN2	565	1.20	0.88300	0.10473	642.0
IRA1512_119.FIN2	888	3.33	1.05470	0.12117	737.2
IRA1512_120.FIN2	91.7	2.02	1.42300	0.14970	912.0
IRA_1514_1.FIN2	46.8	1.24	0.89300	0.10010	614.9
IRA_1514_2.FIN2	180.9	1.13	0.24100	0.03307	209.7
IRA_1514_3.FIN2	196	0.77	1.64200	0.16350	996.0

IRA_1514_4.FIN2	161.6	1.24	0.81100	0.09520	585.9
IRA_1514_5.FIN2	306.6	4.63	0.67500	0.07890	489.0
IRA_1514_6.FIN2	394	2.00	10.92000	0.45720	2574.0
IRA_1514_7.FIN2	308	1.82	1.50300	0.15090	1016.0
IRA_1514_8.FIN2	132.2	2.02	1.25200	0.13410	811.4
IRA_1514_9.FIN2	891	13.80	9.23000	0.35950	2683.0
IRA_1514_10.FIN2	300	0.69	0.25080	0.03641	230.5
IRA_1514_11.FIN2	162.5	1.26	9.66000	0.41800	2519.0
IRA_1514_12.FIN2	398	1.33	5.28200	0.33590	1861.0
IRA_1514_13.FIN2	194	2.06	0.75900	0.09210	567.9
IRA_1514_14.FIN2	488	0.86	0.25800	0.03708	234.7
IRA_1514_15.FIN2	154	2.83	0.97300	0.11150	681.3
IRA_1514_16.FIN2	196	0.98	0.83200	0.10160	623.6
IRA_1514_17.FIN2	228.3	0.59	0.81200	0.09420	580.3
IRA_1514_18.FIN2	84.1	0.42	4.74800	0.28590	1929.0
IRA_1514_19.FIN2	130	1.14	1.73900	0.17240	1011.0
IRA_1514_20.FIN2	67.2	0.51	1.82500	0.17660	1041.0
IRA_1514_21.FIN2	680	0.72	0.26010	0.03722	235.6
IRA_1514_22.FIN2	368	1.62	1.82300	0.17610	1054.0
IRA_1514_23.FIN2	405	1.84	4.44000	0.28120	1858.0
IRA_1514_24.FIN2	182.7	2.15	1.45900	0.14840	967.0
IRA_1514_25.FIN2	288	5.88	0.85500	0.10190	625.0
IRA_1514_26.FIN2	531	0.77	0.25600	0.03638	230.4
IRA_1514_27.FIN2	268	4.88	0.95700	0.11215	685.2
IRA_1514_28.FIN2	86.7	1.61	1.32700	0.14290	853.0
IRA_1514_29.FIN2	87.5	2.64	0.87700	0.10420	638.7
IRA_1514_30.FIN2	65	3.14	0.90700	0.10700	655.3
IRA_1514_31.FIN2	99.9	3.03	1.23700	0.12830	778.0
IRA_1514_32.FIN2	124.9	0.86	1.20000	0.12750	774.0
IRA_1514_33.FIN2	383	5.40	0.97800	0.11270	688.0
IRA_1514_34.FIN2	820	12.80	1.04300	0.11760	716.0

IRA_1514_35.FIN2	590	4.82	0.79800	0.09760	600.0
IRA_1514_36.FIN2	305	2.15	1.14600	0.12830	778.9
IRA_1514_37.FIN2	293.2	9.84	4.64800	0.28750	1900.0
IRA_1514_38.FIN2	232	0.76	0.73900	0.08990	554.0
IRA_1514_39.FIN2	169.1	1.23	0.89200	0.10750	658.2
IRA_1514_40.FIN2	100.6	3.51	0.94100	0.11050	675.5
IRA_1514_41.FIN2	1179	9.77	2.51500	0.18740	1578.0
IRA_1514_42.FIN2	60.3	1.71	1.66600	0.16520	970.0
IRA_1514_43.FIN2	37	11.30	0.87600	0.10560	647.0
IRA_1514_44.FIN2	136.9	2.56	1.01900	0.11850	721.9
IRA_1514_45.FIN2	338.5	5.66	0.93890	0.10950	669.9
IRA_1514_46.FIN2	307	2.98	0.55410	0.07048	439.0
IRA_1514_47.FIN2	23.8	2.88	1.62800	0.16850	943.0
IRA_1514_48.FIN2	320.1	0.96	0.24560	0.03226	204.6
IRA_1514_49.FIN2	591	0.89	0.25710	0.03721	235.5
IRA_1514_50.FIN2	243	1.13	1.64500	0.16650	979.0
IRA_1514_51.FIN2	1202	0.73	0.23630	0.03196	202.8
IRA_1514_52.FIN2	131.6	1.51	1.61700	0.16110	1007.0
IRA_1514_53.FIN2	206	3.41	0.63600	0.07380	459.0
IRA_1514_54.FIN2	450	2.21	1.23500	0.13370	808.5
IRA_1514_55.FIN2	72.3	0.87	1.11700	0.12550	763.0
IRA_1514_56.FIN2	218	1.03	1.36400	0.14660	836.0
IRA_1514_57.FIN2	129.2	1.17	0.85900	0.10220	627.2
IRA_1514_58.FIN2	539	0.79	0.25830	0.03552	225.0
IRA_1514_59.FIN2	360.3	0.93	0.25730	0.03676	232.7
IRA_1514_60.FIN2	320	1.13	0.26350	0.03744	236.9
IRA_1514_61.FIN2	533	4.42	1.26200	0.12960	786.0
IRA_1514_63.FIN2	460.5	1.02	0.25270	0.03519	222.9
IRA_1514_64.FIN2	240.1	2.71	1.03500	0.11630	709.2
IRA_1514_65.FIN2	709	5.34	0.80600	0.09580	589.9
IRA_1514_66.FIN2	117.4	1.28	11.00600	0.47750	2524.0

IRA_1514_67.FIN2	194.5	0.96	1.67100	0.16510	995.0
IRA_1514_68.FIN2	80	0.86	1.00800	0.11680	711.9
IRA_1514_69.FIN2	294	3.27	5.34500	0.33970	1871.0
IRA_1514_70.FIN2	353	1.35	0.97200	0.10690	654.0
IRA_1514_71.FIN2	46.32	1.92	0.98700	0.11030	674.0
IRA_1514_72.FIN2	73.2	2.91	0.82600	0.10000	614.3
IRA_1514_73.FIN2	773	11.10	10.02000	0.45360	2469.0
IRA_1514_74.FIN2	110	1.29	4.71200	0.30760	1811.0
IRA_1514_75.FIN2	166	2.86	5.81000	0.35600	1920.0
IRA_1514_76.FIN2	87.5	0.63	0.85200	0.09640	593.0
IRA_1514_77.FIN2	164	1.83	0.66100	0.08510	526.6
IRA_1514_78.FIN2	337	1.89	0.88500	0.10430	641.3
IRA_1514_79.FIN2	155	2.31	1.22700	0.13400	810.4
IRA_1514_80.FIN2	258.3	3.03	0.67200	0.08338	516.2
IRA_1514_81.FIN2	190	1.68	1.46400	0.15290	911.0
IRA_1514_82.FIN2	545	0.77	0.24830	0.03588	227.2
IRA_1514_83.FIN2	342	3.35	9.63900	0.41350	2546.0
IRA_1514_84.FIN2	132	7.69	1.41400	0.14220	991.0
IRA_1514_85.FIN2	550	6.80	1.49500	0.15520	917.0
IRA_1514_86.FIN2	262.7	1.78	26.52000	0.67630	3385.0
IRA_1514_87.FIN2	60	1.62	1.00700	0.10100	DISC
IRA_1514_88.FIN2	456	1.19	5.55800	0.34800	1897.0
IRA_1514_89.FIN2	1203	7.87	0.79780	0.09583	589.9
IRA_1514_90.FIN2	93.1	1.57	1.55900	0.16130	912.0
IRA_1514_91.FIN2	671	0.69	0.25920	0.03718	235.3
IRA_1514_93.FIN2	80.6	0.62	0.71500	0.08920	550.0
IRA_1514_94.FIN2	310	0.99	0.26230	0.03731	236.1
IRA_1514_95.FIN2	357	1.01	0.25390	0.03646	230.8
IRA_1514_96.FIN2	125.3	1.17	6.75000	0.31790	2398.0
IRA_1514_97.FIN2	212.2	1.52	4.73200	0.28860	1945.0
IRA_1514_98.FIN2	773	3.93	0.49800	0.06090	382.5

IRA_1514_98.FIN2	368.6	2.35	0.70600	0.08530	528.0
IRA_1514_99.FIN2	43.2	0.42	5.43000	0.32550	1949.0
IRA_1514_100.FIN2	230	40.60	0.77600	0.09502	585.1
IRA_1514_101.FIN2	195.6	1.26	1.56400	0.15700	999.0
IRA_1514_102.FIN2	124.1	0.68	5.97900	0.34040	2050.0
IRA_1514_103.FIN2	66.5	0.52	1.11200	0.12550	761.9
IRA_1514_104.FIN2	428.5	3.08	0.55830	0.07116	443.1
IRA_1514_105.FIN2	1201	0.89	0.19470	0.02598	165.4
IRA_1514_106.FIN2	466	0.85	0.24080	0.03431	217.5
IRA_1514_107.FIN2	12.59	0.77	0.82500	0.09580	589.0
IRA_1514_108.FIN2	248.6	2.21	0.84600	0.10170	624.0
IRA_1514_109.FIN2	380	2.52	1.42500	0.14940	932.0
IRA_1514_109.FIN2	328	1.69	0.84400	0.08860	DISC
IRA_1514_110.FIN2	338	31.90	1.07700	0.12230	743.0
IRA_1514_111.FIN2	191	0.77	0.84000	0.10030	615.7
IRA_1514_112.FIN2	155	1.03	0.86200	0.10260	629.7
IRA_1514_113.FIN2	552	0.75	0.25090	0.03622	229.3
IRA_1514_114.FIN2	423	2.81	0.84400	0.09990	613.8
IRA_1514_115.FIN2	173.3	2.03	1.17800	0.12890	781.0
IRA_1514_116.FIN2	270	6.18	0.70500	0.08500	525.9
IRA_1514_118.FIN2	268.8	0.82	6.04800	0.35960	1977.0
IRA_1514_119.FIN2	115.4	2.72	1.01200	0.11420	697.1
IRA_1514_120.FIN2	449	0.86	0.24820	0.03683	233.1
IRA_1511_1.FIN2	124	5.42	4.97800	0.28330	2074.0
IRA_1511_1.FIN3	428	5.08	0.35600	0.04820	303.4
IRA_1511_1.FIN4	189.7	1.86	0.49100	0.06190	387.0
IRA_1511_1.FIN5	297.7	5.86	0.57870	0.07420	461.0
IRA_1511_1.FIN6	919	10.80	0.48900	0.06470	404.0
IRA_1511_1.FIN7	440	1.31	0.35230	0.04526	285.3
IRA_1511_1.FIN8	228.6	4.34	0.54300	0.06817	425.1
IRA_1511_1.FIN9	111	2.21	0.71700	0.08780	543.0

IRA_1511_1.FIN10	531	6.85	8.99900	0.41400	2428.0
IRA_1511_1.FIN11	183.9	2.84	0.67400	0.08047	498.9
IRA_1511_1.FIN12	371	1.70	0.36500	0.04946	311.2
IRA_1511_1.FIN13	34.1	0.81	0.35500	0.04650	293.2
IRA_1511_1.FIN14	278.7	1.83	0.07740	0.01115	71.4
IRA_1511_1.FIN15	566	6.25	0.57800	0.06990	435.0
IRA_1511_1.FIN16	196.8	1.67	0.85700	0.10240	629.0
IRA_1511_1.FIN17	577	46.00	0.48670	0.06351	396.9
IRA_1511_1.FIN18	546	48.00	0.44500	0.05880	368.4
IRA_1511_1.FIN19	218	13.53	0.58100	0.07610	473.0
IRA_1511_1.FIN20	495	4.34	0.29710	0.04150	262.1
IRA_1511_1.FIN21	1001	3.08	0.33600	0.04548	286.7
IRA_1511_1.FIN22	304	1.81	0.17400	0.02458	156.5
IRA_1511_1.FIN23	351	1.77	4.12100	0.29090	1664.0
IRA_1511_1.FIN24	448	1.85	0.36860	0.05050	317.4
IRA_1511_1.FIN25	667	1.51	0.35590	0.04934	310.4
IRA_1511_1.FIN26	906	2.75	0.16940	0.02497	159.0
IRA_1511_1.FIN27	300	2.03	0.25890	0.03812	241.1
IRA_1511_1.FIN28	148.7	1.12	0.87100	0.10100	620.0
IRA_1511_1.FIN29	315	2.78	0.21900	0.02920	185.8
IRA_1511_1.FIN30	110.5	1.47	0.37800	0.05160	324.5
IRA_1511_1.FIN31	465	29.50	0.50500	0.06410	400.0
IRA_1511_1.FIN32	626	9.43	0.40900	0.05030	316.0
IRA_1511_1.FIN33	269.6	6.87	0.63000	0.08150	505.0
IRA_1511_1.FIN34	279	2.47	1.20500	0.12970	786.0
IRA_1511_1.FIN35	164	2.16	0.78700	0.08950	553.0
IRA_1511_1.FIN36	1188	11.50	0.14700	0.02049	130.8
IRA_1511_1.FIN37	469	7.24	0.35780	0.04932	310.4
IRA_1511_1.FIN38	962	3.80	0.81700	0.09820	604.1
IRA_1511_1.FIN39	367	14.20	0.24700	0.03110	DISC
IRA_1511_1.FIN40	185.6	5.35	0.41540	0.05490	344.3

IRA_1511_1.FIN41	1010	13.19	0.24270	0.03197	202.9
IRA_1511_1.FIN42	225.9	9.54	0.57800	0.07300	454.0
IRA_1511_1.FIN43	843	48.70	0.34900	0.04530	285.5
IRA_1511_1.FIN44	369	19.90	0.60900	0.07600	471.9
IRA_1511_1.FIN45	298.4	1.03	1.49600	0.14680	1024.0
IRA_1511_1.FIN46	761	91.90	0.29720	0.04040	256.0
IRA_1511_1.FIN47	598	1.09	0.72400	0.08630	534.0
IRA_1511_1.FIN48	970	52.00	0.06150	0.00737	DISC
IRA_1511_1.FIN49	215	1.45	0.36630	0.05094	320.3
IRA_1511_1.FIN50	54.2	0.74	0.88500	0.10330	633.0
IRA_1511_1.FIN51	361	2.30	0.24360	0.03363	213.2
IRA_1511_1.FIN52	178	4.98	0.56400	0.07330	456.2
IRA_1511_1.FIN53	72.2	0.78	1.68400	0.16510	1007.0
IRA_1511_1.FIN54	620	13.30	0.07000	0.00932	DISC
IRA_1511_1.FIN55	907.7	0.95	0.20060	0.02994	190.2
IRA_1511_1.FIN56	347	16.00	0.34300	0.04730	297.7
IRA_1511_1.FIN57	900	7.22	0.32300	0.04290	271.0
IRA_1511_1.FIN58	564	4.31	0.39110	0.05291	332.4
IRA_1511_1.FIN60	650	34.80	0.07000	0.00789	DISC
IRA_1511_1.FIN61	378	5.36	0.08850	0.01180	DISC
IRA_1511_1.FIN62	41	0.92	0.27900	0.03695	233.8
IRA_1511_1.FIN63	376	2.41	0.57600	0.07060	439.7
IRA_1511_1.FIN64	200.1	1.98	0.51500	0.06580	410.9
IRA_1511_1.FIN65	391	1.42	0.06890	0.00903	DISC
IRA_1511_1.FIN66	2440	87.00	0.06900	0.01010	DISC
IRA_1511_1.FIN67	820	3.45	0.54000	0.06710	418.9
IRA_1511_1.FIN68	355	1.58	0.76100	0.09380	577.9
IRA_1511_1.FIN69	590	133.00	0.35900	0.04908	308.9
IRA_1511_1.FIN70	158.9	2.09	1.07900	0.12280	747.0
IRA_1511_1.FIN71	284	2.27	0.05250	0.00810	52.0
IRA_1511_1.FIN72	110.1	1.16	1.43800	0.14810	1000.0

IRA_1511_1.FIN73	318.2	5.79	0.57630	0.07366	458.1
IRA_1511_1.FIN74	175	1.51	1.10100	0.12250	744.0
IRA_1511_1.FIN75	335	1.60	0.07400	0.01143	73.2
IRA_1511_1.FIN76	2320	11.90	0.08800	0.00826	DISC
IRA_1511_1.FIN77	1122	4.10	0.08810	0.01297	83.0
IRA_1511_1.FIN78	179	1.02	0.18360	0.02577	164.0
IRA_1511_1.FIN79	38.1	1.12	10.92000	0.45700	2607.0
IRA_1511_1.FIN80	258	1.31	0.27040	0.03789	239.7
IRA_1511_1.FIN81	381	2.66	0.37330	0.05117	321.7
IRA_1511_1.FIN82	1039	1.45	0.79600	0.09740	599.0
IRA_1511_1.FIN83	1530	15.67	0.18400	0.02356	DISC
IRA_1511_1.FIN84	784	7.83	0.50200	0.06630	414.1
IRA_1511_1.FIN85	685.5	2.10	0.69800	0.08670	535.9
IRA_1511_1.FIN86	49.5	2.45	11.01000	0.48400	2527.0
IRA_1511_1.FIN87	689	25.30	0.08300	0.00957	DISC
IRA_1511_1.FIN88	527	3.89	0.18130	0.02520	160.3
IRA_1511_1.FIN89	197.8	1.33	0.40900	0.05520	346.5
IRA_1511_1.FIN90	801	81.00	0.17000	0.02460	156.0
IRA_1511_1.FIN91	36.5	1.87	0.90400	0.10350	635.0
IRA_1511_1.FIN92	783	3.53	0.31780	0.04439	280.0
IRA_1511_1.FIN93	290.1	5.34	0.58980	0.07496	465.9
IRA_1511_1.FIN94	680	0.94	0.09140	0.01303	83.5
IRA_1511_1.FIN95	124.1	1.15	0.34800	0.04760	299.8
IRA_1511_1.FIN96	677	13.90	0.13730	0.01950	124.3
IRA_1511_1.FIN97	325	1.85	0.31560	0.04410	278.3
IRA_1511_1.FIN98	406	21.23	0.24800	0.03170	DISC
IRA_1511_1.FIN99	256	5.11	0.64800	0.08020	497.6
IRA_1511_1.FIN100	123	0.89	6.10300	0.35830	1986.0
IRA_1511_1.FIN101	802	4.48	0.17600	0.02360	150.2
IRA_1511_1.FIN102	840	3.02	0.27200	0.03527	223.4
IRA_1511_1.FIN103	476.3	4.15	0.35200	0.04895	308.1

IRA_1511_1.FIN104	101.4	1.16	0.23710	0.03425	217.1
IRA_1511_1.FIN105	200	5.06	0.49600	0.06360	397.0
IRA_1511_1.FIN106	527	1.76	0.36500	0.04990	313.9
IRA_1511_1.FIN107	662	8.50	0.26000	0.03140	DISC
IRA_1511_1.FIN108	293	2.46	0.63400	0.08060	504.0
IRA_1511_1.FIN109	125.1	1.00	0.87100	0.10380	636.0
IRA_1511_1.FIN110	872	19.57	0.24100	0.03060	DISC
IRA_1511_1.FIN111	250	13.62	0.47900	0.06230	389.4
IRA_1511_1.FIN112	474	2.80	0.59900	0.07685	477.3
IRA_1511_1.FIN113	744	1.21	0.06010	0.00878	56.4
IRA_1511_1.FIN114	631	1.32	0.05730	0.00874	56.1
IRA_1511_1.FIN115	411	70.00	0.07260	0.00853	DISC
IRA_1511_1.FIN116	164.3	3.41	0.87000	0.08960	DISC
IRA_1511_1.FIN117	244	1.85	0.75600	0.08840	546.0
IRA_1511_1.FIN118	608	20.60	0.41400	0.05280	331.6
IRA_1511_1.FIN119	260	4.33	0.60400	0.07520	468.0
IRA_1511_1.FIN120	87.4	1.46	0.85700	0.10230	628.0
IRA_1511_1.FIN121	171	1.35	0.36720	0.05065	318.5
IRA_1511_1.FIN122	370	1.89	0.35040	0.04752	299.2
IRA_1511_1.FIN123	106.4	0.50	10.00000	0.45220	2472.0
IRA_1511_1.FIN124	220.1	9.92	0.38410	0.05229	328.5
IRA_1511_1.FIN125	528	1.13	0.05910	0.00876	56.2
IRA_1511_1.FIN126	2870	2.39	0.25100	0.03270	208.0
IRA_1511_1.FIN127	417	1.29	0.37570	0.05235	328.9
IRA_1511_1.FIN128	208.4	2.14	0.78800	0.09020	556.0
IRA_1511_1.FIN129	243	6.07	0.54430	0.06982	435.0
IRA_1511_1.FIN130	103.4	0.87	0.31100	0.04499	283.6
IRA_1511_1.FIN131	1003	19.70	0.08520	0.01324	84.8
IRA_1511_1.FIN132	474	5.77	0.17700	0.02532	161.2
IRA_1511_1.FIN133	600	5.62	0.13350	0.01768	DISC
IRA_1511_1.FIN134	103.7	0.57	0.65500	0.08190	507.3

IRA_1511_1.FIN135	732	14.86	0.08600	0.01260	80.7
IRA_1511_1.FIN136	693	78.40	0.35310	0.04805	302.5
IRA_1511_1.FIN137	942	61.60	0.47000	0.06340	396.5
IRA_1511_1.FIN138	698	15.36	0.88900	0.10260	629.8
IRA_1511_1.FIN139	639	23.30	0.55300	0.06840	426.2
IRA_1511_1.FIN140	293	2.02	0.75600	0.09097	561.2
IRA_1511_1.FIN141	722	2.03	0.40900	0.05660	355.1
IRA_1511_1.FIN142	1120	10.30	0.10070	0.01470	94.2
IRA_1511_1.FIN143	471	1.08	0.24570	0.03367	213.5
IRA_1511_1.FIN144	253	2.09	0.35040	0.04596	289.6
IRA_1511_1.FIN145	504	9.83	0.15800	0.02090	DISC
IRA_1511_1.FIN146	89.2	1.22	0.34800	0.04830	304.2
IRA_1511_1.FIN147	801	1.54	0.36270	0.04938	310.7
IRA_1511_1.FIN148	730	43.00	0.06400	0.00900	DISC
IRA_1511_1.FIN149	376	0.75	0.35720	0.04827	303.9
IRA_1511_1.FIN150	684	1.07	0.06020	0.00898	57.6
IRA_1511_1.FIN151	193.3	1.34	0.37400	0.05250	329.6
IRA_1511_1.FIN152	581	1.19	0.73500	0.09020	556.0
IRA_1511_1.FIN153	1043	25.60	0.17500	0.02217	DISC
IRA_1511_1.FIN154	505	3.90	0.48480	0.06210	388.3
IRA_1511_1.FIN155	387	2.16	0.36820	0.04984	313.5
IRA_1511_1.FIN156	179	1.02	1.10100	0.12240	744.0
IRA_1511_1.FIN157	96.1	1.45	8.47000	0.35300	2593.0
IRA_1511_1.FIN159	214	5.10	0.57600	0.07400	460.3
IRA_1511_1.FIN160	444	1.66	0.68450	0.08558	529.3
IRA_1511_1.FIN161	653	1.01	0.06000	0.00883	56.6
IRA_1511_1.FIN162	371	3.44	0.26470	0.03543	224.5
IRA_1513_1.FIN2	2365	60.60	0.06280	0.00904	58.0
IRA_1513_1.FIN3	430	5.61	0.38700	0.04870	307.0
IRA_1513_1.FIN4	2820	47.40	0.05360	0.00744	47.8
IRA_1513_1.FIN5	449	5.23	0.20800	0.02660	DISC

IRA_1513_1.FIN6	274	1.86	0.52000	0.06780	422.8
IRA_1513_1.FIN7	121.2	1.02	0.87500	0.10570	647.5
IRA_1513_1.FIN8	903	64.10	0.04840	0.00662	DISC
IRA_1513_1.FIN9	771	38.10	0.08060	0.01078	DISC
IRA_1513_1.FIN10	216.3	13.54	0.14340	0.01887	DISC
IRA_1513_1.FIN11	170	1.17	0.57300	0.06930	432.0
IRA_1513_1.FIN12	205	3.79	1.85600	0.17650	1097.0
IRA_1513_1.FIN13	1650	23.00	0.10280	0.01403	89.8
IRA_1513_1.FIN14	252.7	3.11	0.45100	0.05792	363.0
IRA_1513_1.FIN15	519	2.68	0.34610	0.04814	303.1
IRA_1513_1.FIN16	1087	56.70	0.05410	0.00739	DISC
IRA_1513_1.FIN17	307.2	1.06	7.38200	0.37320	2261.0
IRA_1513_1.FIN18	870	4.67	0.24750	0.03185	202.1
IRA_1513_1.FIN19	98.6	0.96	0.84600	0.10260	629.7
IRA_1513_1.FIN20	2260	44.70	0.07130	0.00934	DISC
IRA_1513_1.FIN21	982	20.90	0.05590	0.00703	DISC
IRA_1513_1.FIN22	101	22.10	0.79900	0.09280	573.0
IRA_1513_1.FIN23	233	4.69	0.96100	0.11090	678.1
IRA_1513_1.FIN24	208.3	1.13	0.72400	0.08870	548.0
IRA_1513_1.FIN25	207.9	1.02	0.73000	0.08920	550.6
IRA_1513_1.FIN26	143.4	2.17	3.79900	0.23990	1875.0
IRA_1513_1.FIN27	198.5	1.77	0.36250	0.05038	316.8
IRA_1513_1.FIN28	343.9	4.13	0.95300	0.10500	644.0
IRA_1513_1.FIN29	428	4.43	0.23300	0.03090	196.3
IRA_1513_1.FIN30	775	3.98	0.85200	0.09450	582.0
IRA_1513_1.FIN31	253.6	3.30	0.36260	0.05042	317.1
IRA_1513_1.FIN32	1004	108.00	0.06890	0.00890	DISC
IRA_1513_1.FIN33	46.1	2.81	0.68500	0.07710	479.0
IRA_1513_1.FIN34	983	29.00	0.08100	0.01098	DISC
IRA_1513_1.FIN35	608.7	4.44	0.22820	0.02918	DISC
IRA_1513_1.FIN36	239	3.11	0.56200	0.07286	453.3

IRA_1513_1.FIN37	176.6	2.35	0.88200	0.10350	634.9
IRA_1513_1.FIN38	162	1.95	0.86700	0.10270	630.0
IRA_1513_1.FIN39	2208	9.73	0.12000	0.01693	108.2
IRA_1513_1.FIN40	413	2.59	0.33560	0.04639	292.3
IRA_1513_1.FIN41	185	1.00	0.84600	0.09910	608.8
IRA_1513_1.FIN42	975	11.60	0.23940	0.03031	DISC
IRA_1513_1.FIN44	173.2	5.71	0.55940	0.07230	449.9
IRA_1513_1.FIN45	218	1.68	4.89000	0.31100	1866.0
IRA_1513_1.FIN46	1860	29.20	0.06370	0.00917	58.8
IRA_1513_1.FIN47	908	6.94	0.22750	0.03182	201.9
IRA_1513_1.FIN48	143.1	3.60	0.52600	0.06850	426.8
IRA_1513_1.FIN49	873	23.60	0.11160	0.01465	DISC
IRA_1513_1.FIN50	148.5	3.80	0.51200	0.06560	410.0
IRA_1513_1.FIN51	21.3	1.38	1.52900	0.16350	810.0
IRA_1513_1.FIN52	302.2	7.00	0.54120	0.06900	430.2
IRA_1513_1.FIN53	1044	17.42	0.07150	0.00986	63.2
IRA_1513_1.FIN54	233	1.95	0.35500	0.04753	299.3
IRA_1513_1.FIN55	286	1.11	1.26100	0.13510	816.0
IRA_1513_1.FIN56	139	1.16	1.41000	0.14200	993.0
IRA_1513_1.FIN57	991	6.23	0.26400	0.03180	DISC
IRA_1513_1.FIN58	318	2.73	0.78800	0.09010	556.0
IRA_1513_1.FIN59	52.8	2.11	0.67300	0.08490	525.0
IRA_1513_1.FIN60	1170	15.90	0.09440	0.01329	85.1
IRA_1513_1.FIN61	144.6	3.19	0.52700	0.06910	431.8
IRA_1513_1.FIN62	27.6	0.48	1.35800	0.13950	841.0
IRA_1513_1.FIN63	69.9	1.27	1.60400	0.15330	1092.0
IRA_1513_1.FIN64	537	3.85	0.37950	0.04970	312.6
IRA_1513_1.FIN65	140.1	5.61	0.48600	0.06250	391.0
IRA_1513_1.FIN66	133.7	1.69	5.82000	0.34280	1997.0
IRA_1513_1.FIN67	507	7.36	0.28600	0.03590	DISC
IRA_1513_1.FIN68	127.3	1.14	0.60400	0.07010	436.7

IRA_1513_1.FIN69	138	0.36	1.59400	0.16020	970.0
IRA_1513_1.FIN70	154.1	0.92	1.69300	0.16590	1044.0
IRA_1513_1.FIN71	1410	24.00	0.09990	0.01363	87.3
IRA_1513_1.FIN72	137.7	3.74	0.56400	0.07180	446.9
IRA_1513_1.FIN73	41.05	3.55	1.89000	0.18360	1062.0
IRA_1513_1.FIN74	869	83.00	0.06190	0.00940	DISC
IRA_1513_1.FIN75	116.4	13.50	0.99400	0.09360	569.0
IRA_1513_1.FIN76	1180	31.60	0.10900	0.01398	DISC
IRA_1513_1.FIN77	105.4	2.54	0.83500	0.09550	588.0
IRA_1513_1.FIN78	684	10.55	0.25010	0.03200	DISC
IRA_1513_1.FIN80	242	1.05	1.56100	0.15710	1003.0
IRA_1513_1.FIN81	158	0.68	0.80800	0.09950	611.3
IRA_1513_1.FIN82	42.1	0.64	1.49100	0.15410	935.0
IRA_1513_1.FIN83	471	3.14	0.55650	0.07138	444.4
IRA_1513_1.FIN84	278.9	1.36	9.38000	0.37860	2640.0
IRA_1513_1.FIN85	53.5	1.71	0.88200	0.09060	DISC
IRA_1513_1.FIN86	219.5	2.11	0.77500	0.09460	582.0
IRA_1513_1.FIN87	1143	14.84	0.12060	0.01504	DISC
IRA_1513_1.FIN88	419	15.30	0.44600	0.05780	362.0
IRA_1513_1.FIN89	153.3	1.17	1.35900	0.13860	837.0
IRA_1513_1.FIN90	1119	55.10	0.07010	0.00784	DISC
IRA_1513_1.FIN91	597	34.80	0.11920	0.01543	DISC
IRA_1513_1.FIN92	206	3.51	0.68100	0.07940	493.0
IRA_1513_1.FIN93	320	1.66	0.36580	0.05003	314.7
IRA_1513_1.FIN94	1427	157.00	0.07200	0.01020	65.4
IRA_1513_1.FIN95	274	8.49	0.48900	0.06240	390.0
IRA_1513_1.FIN96	221	8.93	0.54560	0.07040	438.4
IRA_1513_1.FIN97	765	111.00	0.07800	0.00835	DISC
IRA_1513_1.FIN98	175	4.50	0.67100	0.08070	500.0
IRA_1513_1.FIN99	126	1.24	1.76900	0.17360	1051.0
IRA_1513_1.FIN100	197.3	1.62	0.58400	0.07470	464.2

IRA_1513_1.FIN101	96.1	0.47	1.61000	0.16020	1012.0
IRA_1513_1.FIN102	229	1.13	1.08400	0.11550	704.0
IRA_1513_1.FIN103	171.9	2.21	1.13400	0.12190	741.0
IRA_1513_1.FIN104	1095	16.50	0.09510	0.01298	83.2
IRA_1513_1.FIN105	44	0.93	0.66900	0.07940	493.0
IRA_1513_1.FIN106	1709	20.60	0.11720	0.01456	DISC
IRA_1513_1.FIN107	104.9	1.88	0.92300	0.10680	654.0
IRA_1513_1.FIN108	420	2.50	0.35410	0.04904	308.6
IRA_1513_1.FIN109	207.2	10.12	0.30200	0.03720	DISC
IRA_1513_1.FIN110	130	1.17	1.29800	0.13310	805.0
IRA_1513_1.FIN111	150.6	1.04	4.97700	0.32300	1847.0
IRA_1513_1.FIN112	238	2.54	0.52500	0.06590	412.9
IRA_1513_1.FIN113	2377	293.00	0.04720	0.00694	44.6
IRA_1513_1.FIN114	1798	81.00	0.07250	0.00970	DISC
IRA_1513_1.FIN115	82.5	1.39	0.81900	0.10080	618.8
IRA_1513_1.FIN116	4690	406.00	0.05450	0.00823	52.8
IRA_1513_1.FIN117	94.1	0.90	1.09000	0.12280	746.0
IRA_1513_1.FIN118	578	19.20	0.09150	0.01202	DISC
IRA_1513_1.FIN119	123	2.72	0.73700	0.08750	540.6
IRA_1513_1.FIN120	53	0.83	5.49000	0.30900	2104.0
IRA_1513_1.FIN121	142.1	4.75	0.84300	0.10120	621.0
IRA_1513_1.FIN122	830	22.00	0.17100	0.01940	DISC
IRA_1513_1.FIN123	587	3.74	0.43600	0.05350	335.6
IRA_1513_1.FIN124	356	7.38	0.61800	0.07190	447.0
IRA_1513_1.FIN125	1033	35.90	0.09160	0.01197	DISC
IRA_1513_1.FIN126	158.3	2.20	0.54970	0.07207	448.6
IRA_1513_1.FIN128	122	3.84	1.54200	0.15630	993.0
IRA_1513_1.FIN129	244	2.49	0.89900	0.10670	653.8
IRA_1513_1.FIN130	221	6.04	0.23800	0.02920	DISC
IRA_1513_1.FIN131	114.2	3.27	0.53500	0.06540	408.1
IRA_1513_1.FIN132	212.3	1.96	0.56100	0.07090	441.2

IRA_1513_1.FIN133	1103	216.00	0.04650	0.00728	46.7
IRA_1513_1.FIN134	74	5.22	1.00700	0.11310	691.0
IRA_1513_1.FIN135	690	35.50	0.08590	0.01188	76.1
IRA_1513_1.FIN136	793	4.87	0.30700	0.03550	DISC
IRA_1513_1.FIN137	244	2.87	0.56400	0.07014	436.9
IRA_1513_1.FIN138	1970	172.00	0.04560	0.00703	45.2
IRA_1513_1.FIN139	765	211.00	0.04840	0.00701	45.0
IRA_1513_1.FIN140	207	1.09	0.26900	0.03598	227.8
IRA_1513_1.FIN141	1490	29.50	0.09150	0.01283	82.2
IRA_1513_1.FIN142	194	3.13	0.50600	0.06620	413.5
IRA_1513_1.FIN143	158.8	2.85	0.55830	0.07239	450.5
IRA_1513_1.FIN144	572	4.26	0.23670	0.03160	200.6
IRA_1513_1.FIN145	267	2.03	0.37420	0.05113	321.4
IRA_1513_1.FIN146	136.7	1.05	13.47000	0.51660	2734.0
IRA_1513_1.FIN147	237	1.52	0.26930	0.03752	237.4
IRA_1513_1.FIN148	197	6.02	0.54890	0.07131	444.0